Vancomycin-loaded nanobubbles: A new platform for controlled antibiotic delivery against methicillin-resistant Staphylococcus aureus infections

Elsevier Editorial System(tm) for
International Journal of Pharmaceutics
Manuscript Draft

Manuscript Number: IJP-D-16-02774R1

Title: Vancomycin-loaded nanobubbles: a new platform for controlled antibiotic delivery against methicillin-resistant Staphylococcus aureus infections.

Article Type: Research Paper

Section/Category: Pharmaceutical Nanotechnology

Keywords: nanobubbles, vancomycin, methicillin-resistant Staphylococcus aureus, ultrasound, prolonged release

Corresponding Author: Dr. Roberta Cavalli,

Corresponding Author's Institution: University of Turin

First Author: Monica Argenziano

Order of Authors: Monica Argenziano; Giuliana Banche; Anna Luganini; Nicole Finesso; Valeria Allizond; Giulia Rossana Gulino; Amina Khadjavi; Rita Spagnolo; Vivian Tullio; Giuliana Giribaldi; Caterina Guiot; Anna Maria Cuffini; Mauro Prato; Roberta Cavalli

Abstract: Vancomycin (Vm) currently represents the gold standard against methicillin-resistant Staphylococcus aureus (MRSA) infections. However, it is associated with low oral bioavailability, formulation stability issues, and severe side effects upon systemic administration. These drawbacks could be overcome by Vm topical administration if properly encapsulated in a nanocarrier. Intriguingly, nanobubbles (NBs) are responsive to physical external stimuli such as ultrasound (US), promoting drug delivery. In this work, perfluoropentane (PFP)-cored NBs were loaded with Vm by coupling to the outer dextran sulfate shell. Vm-loaded NBs (VmLNBs) displayed ~300 nm sizes, anionic surfaces and good drug encapsulation efficiency. In vitro, VmLNBs showed prolonged drug release kinetics, not accompanied by cytotoxicity on human keratinocytes. Interestingly, VmLNBs were generally more effective than Vm alone in MRSA killing, with VmLNB antibacterial activity being more sustained over time as a result of prolonged drug release profile. Besides, VmLNBs were not internalized by staphylococci, opposite to Vm solution. Further US association promoted drug delivery from VmLNBs through an in vitro model of porcine skin. Taken together, these results support the hypothesis that proper Vm encapsulation in US-responsive NBs might be a promising strategy for the topical treatment of MRSA wound infections.

Cover Letter

Torino, Italy: 14th March 2017

To the Editor

of the International Journal of Pharmaceutics

Dear Editor,

please find attached here the revised version (both marked and clean copies) of our research article titled "Vancomycin-loaded nanobubbles: a new platform for controlled antibiotic delivery against methicillin-resistant *Staphylococcus aureus* infections".

As requested, the manuscript was implemented according to the reviewer's suggestions and all the references were modified according to the journal's author guidelines. Following the reviewer's comments, the image quality was improved for all figures. A rebuttal letter containing our replies to the author(s)'s comments is also attached.

We sincerely hope that you will find the revised version of the manuscript acceptable for publication by the International Journal of Pharmaceutics.

We are looking forward to receiving your feedback.

Kind regards

Prof. Roberta Cavalli

IJP AUTHOR CHECKLIST

Dear Author,

It frequently happens that on receipt of an article for publication, we find that certain elements of the manuscript, or related information, is missing. This is regrettable of course since it means there will be a delay in processing the article while we obtain the missing details.

In order to avoid such delays in the publication of your article, if accepted, could you please run through the list of items below and make sure you have completed the items.

Overall Manuscript Details

- Is this the final revised version? X
- Are all text pages present? X
- Are the corresponding author's postal address, telephone and fax numbers complete on the manuscript? X
- **Have you provided the corresponding author's e-mail address? X**
- **Manuscript type – please check one of the following:**
  - Full-length article X
  - Review article ☐
  - Rapid Communication ☐
  - Note ☐
  - Letter to the Editor ☐
  - Other ☐
- **Manuscript section – paper to be published in:**
  - Pharmaceutical Nanotechnology section X
  - Personalised Medicine section ☐

Manuscript elements

- Short summary/abstract enclosed? X
- 3-6 Keywords enclosed? X
- Complete reference list enclosed? X
- Is the reference list in the correct journal style? X
- Are all references cited in the text present in the reference list? X
- Are all **original** figures cited in the text enclosed? X
  - Electronic artwork format? ----------
- Are figure legends supplied? X
- Are all figures numbered and orientation provided? X
- Are any figures to be printed in colour? ☐
  - If yes, please list which figures here:----------
- If applicable, are you prepared to pay for reproduction in colour? ☐
- Are all tables cited in the text supplied? X

General

- Can you accept pdf proofs sent via e-mail? X

***Response to Reviewers**

Reviewers' comments:

Reviewer #1: Comments:

1. The quality of figures should be greatly improved, especially the graphical abstract, Figure 3 and 6.

We apologize for such an issue. According to the reviewer's suggestion, the image quality was improved for all figures.

2. In line 159, the section 2.2.1., How many ml of dextran sulfate aqueous solutions were added into the Vm solution? What is the solvent of Vm solution? Water or other organic solvents? When centrifuge the unbound Vm, how much is the centrifugal speed? And the centrifugal time also should be provided.

One ml of dextran sulfate aqueous solution at increasing concentrations was added into 1 ml of vancomycin aqueous solution. The centrifugal speed used was 20000 rpm for 15 minutes. The manuscript was implemented with such information (Materials&Methods section, par. 2.2.1).

3. For preparing pre-emulsion containing Epikuron® 200, palmitic acid and PFP, how much g/mg of PFP was used? To prepare polymeric NBs, How many ml of dextran sulfate aqueous solution was added into the PFP emulsion?

The amount of PFP and dextran sulfate used for each nanobubble formulation were 500 μL and 350 μL, respectively. Such information was added in the text (Materials&Methods section, par. 2.2.2).

4. In line 199, for the TEM observation, the type and brand for the TEM equipment should be provided in the text.

The type and brand of the instrument used for TEM analyses (Philips CM10 (Eindhoven, NL)) were added in the text (Materials&Methods section, par. 2.3.1).

5. To measure the loading capacity, the VmLNBs solution was sonicated and centrifuged, and then the supernatant was analyzed. How to validate the VmLNBs were completely broken? Why not use the organic solvent to destroy the structure of the VmLNBs?

The parameters of the used freeze-drying process are severe to maintain the integrity of the nanostructure in the absence of any cryoprotectors. Preliminary experiments were carried out to evaluate by optical microscopy the nanobubble structure and to set a protocol suitable for determining the loading capacity. The manuscript was modified accordingly (Materials&Methods section, par. 2.3.5).

6. In line 285, the unit of centrifugal speed was g, in line 230, the unit is rpm. The author should check them. Some similar expressions also should be uniformed, such as mL and microL.

All units of centrifugal speed as well as those indicating microliters were uniformed throughout the full text.

7. The viscosity of VmLNBs was higher than that of NB. The reason should be explained in the section of "Discussion". Does the change of viscosity affect loading capacity, encapsulation efficiency, physical stability, Vm release, and permeation efficiency?

We apologize for the typing mistake concerning the viscosity value of blank NB formulations. We determined again the viscosity using the Ubbelhode capillary viscosimeter to confirm the data. The viscosity of all NB formulations (i.e. blank NBs, VmLNBs, fluorescent NBs, and fluorescent VmLNBs) did not show any significant changes. A specific sentence was added in the text (Results section par. 3.1).

8. Table 2 can be incorporated in Table 1.

According to the reviewer's suggestion, Table 2 was incorporated in Table1.

Reviewer #2: The development of novel systems for antibiotics is in its infancy as compared to other disease conditions and is receiving increasing interest in the literature. Whilst several nanosystems are being reported for vancomycin, few, if any have been with nanobubbles. Further, transdermal delivery of nanoencapsulated antibiotics is an emerging research area. This paper describes the encapsulation of vancomycin into nanobubbles for ultrasound mediated drug release and also to bypass the stratum corneum to optimize the treatment of wound infections. This proof of concept study is well designed and the potential of this delivery system is demonstrated. The paper is well written with some minor recommendations:

1. Images of the nanobubbles show one with a single nanobubble and another with 2. Ideally an image showing a population representation should be considered.

A TEM image showing a population representation of VmLNBs was added in the Supplementary Information.

2. There are several inconsistencies in the referencing style which need to be corrected.

All the references were modified according to the journal's author guidelines.

3. Pg 18, Line 368. The last sentence is incorrect and needs to be rewritten.

According to the reviewer's suggestion, we changed the sentence as follows: "As shown in Figure 3, the drug resulted much more stable from a chemical point of view when properly incorporated in the nanocarrier (VmLNBs) than as such in solution." (Results section, par. 3.2)

Reviewer #3: Manuscript IJP-D-16-02774 "Vancomycin - loaded nanobubbles: a new platform for controlled...." by Argenziano et al. describes the fabrication, characterization and release capability of polymer shelled droplets loaded with vancomycin.

The manuscript should be implemented according to the following comments:

1) It should be specified whether PFP is liquid.

Perfluoropentane is a perfluorocarbon with a boiling point of 29°C, hence liquid at room temperature. The use of PFP allows liquid droplet generation at room temperature. Then, PFP in nanodroplets can be activated by an external stimulus, like ultrasound, by means of a mechanism called acoustic droplet vaporization, causing the droplet to become a bubble. The sentence was added in the manuscript (Introduction section, lines 117-120).

2) Term "nanobubbles" can be misleading. At room temperature the core of the particles is liquid PFP. Therefore nanobubbles does not describes correctly such particles. It would be more proper the term "nanodroplets" or "nanovescicles"

The formulation is referred to as “nanobubbles” for sake of simplicity (to distinguish them from so-called decafluoropentane-containing nanodroplets, already patented by our group; see Introduction section for more details about those nanodroplets) but we acknowledge that, prior to the application of ultrasound, it would be more precise to use the term “nanodroplets” when the core is constituted of perfluoropentane. This clarification was included in the text (Introduction section, lines 129-132).

3) Figures are not numbered and are very low in resolution (including the graphical abstract). Sometimes they are not readable.

We apologize for the low quality of figures. According to the reviewer’s suggestion, the resolution of all figures was improved. Also, Figures were numbered in accordance to legend numbers.

4) Scheme of the particle differs from the particle description of the graphical abstract in the position of vancomycin, tethered to the external surface of the particle and in the particle shell, respectively.

Vancomycin is included in the polysaccharide shell. For clarity, we modified Figure 1.

5) Viscosity measurements obtained by capillary viscosimetry should be defined. With an Ubbelhode capillary viscometer a relative viscosity, a specific viscosity, an intrinsic viscosity can be obtained. Which one is reported ? All of them have different dimensions from the reported one, i.e. cP. Relative (to solvent) and specific viscosities are dimensionless, intrinsic viscosity has dimension of an inverse of concentration.

With the Ubbelhode capillary viscometer, the time required for the nanosuspension to flow through a capillary of a known diameter of a certain factor (K) between two marked points was measured. By multiplying the time taken, by the factor of the viscometer (0.105), the kinematic viscosity was obtained. The dynamic viscosity was obtained by multiplying kinematic viscosity by density. The cP is the unit of dynamic viscosity in the metric CGS (centimeter-gram-second) system.

6) Vancomycin permeation study puzzled me a lot. The experiment should be conducted at osmotic conditions. To avoid Donnan effects with a charged not diffusible solute, i.e. nanobubbles, a suitable diffusible ionic strength should be used on both the compartments separated by the membrane. According to the given description NaCl 0.9 % w/w has been added only on one compartment. In this conditions other, not controlled contributions affects the diffusion process of vancomycin. In the description of the set up, the concentration of nanobubbles is not reported.

We apologize for the inaccurate description of the experimental setup. For *in vitro* permeation studies, NB samples were prepared in saline solution (NaCl 0.9% w/v). The concentration of NBs in the donor phase was $1x10^{12}$ NBs/ml. All information was added to the text (Materials&Methods section, par. 2.2.2 and 2.5).

7) When ultrasound are applied, it is important to check the behaviour of the "nanobubbles" (nanodroplets) in order to frame the enhanced release. Do "nanobubbles" (naonodroplets) undergo acoustic droplet vaporization? This effect is known to transform droplets into bubbles, thus changing the release of the payload.

Nanobubbles were observed by US standard imaging (MyLab ESAOTE instrument) and they showed a good scattering response, either in the absence or presence of vancomycin. Further investigations are needed to check whether actual vaporization occurred. With regard to the drug release, preliminary experiments showed an enhanced release kinetics after US application.

8) Pg 6 line 115: PFP is liquid or gas ?

Perfluoropentane is liquid at room temperature, having a boiling point of about 29 °C. Therefore, it is gaseous at body temperature (37°C) as such.

9) Pg 15 line 332: why in confocal microscopy imaging, bacteria are dried ?

The drying of bacteria is a step necessary for their staining. After smearing of bacteria on the glass-slide, every staining procedure considers that bacteria have to be air-dried to fix them on the slide and to avoid the subsequent rinsing of the smear during staining procedure, as well as to allow the sample to more readily take up stain(s).

10) Vancomycin hydrochloride is not mentioned in the Material section.

Vancomycin hydrochloride was from Sigma-Aldrich (St Louis, MO). Therefore, it falls into the general sentence “All materials were from Sigma-Aldrich, St Louis, MO, unless those indicated as follows” (first sentence of par. 2.1 in Materials&Methods section).

***Graphical Abstract (for review)**

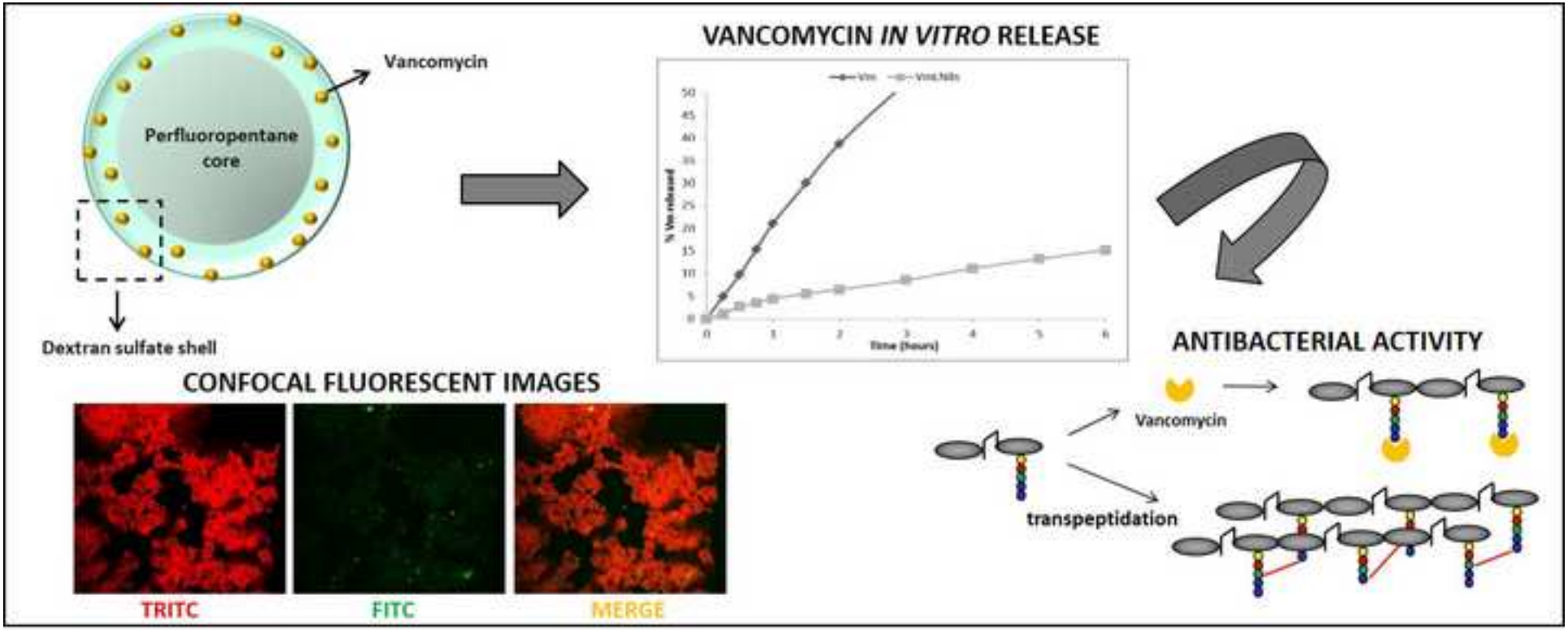

Vancomycin-loaded nanobubbles: a new platform for controlled antibiotic delivery against methicillin-resistant *Staphylococcus aureus* infections.

Monica Argenziano[1], Giuliana Banche[2,*], Anna Luganini[3], Nicole Finesso[4], Valeria Allizond[2], Giulia Rossana Gulino[4], Amina Khadjavi[4,5], Rita Spagnolo[1], Vivian Tullio[2], Giuliana Giribaldi[4], Caterina Guiot[5], Anna Maria Cuffini[2], Mauro Prato[2,5,§], Roberta Cavalli[1, §,*]

[1] *Dipartimento di Scienza e Tecnologia del Farmaco, Università degli Studi di Torino, Torino, Italy*

[2] *Dipartimento di Scienze della Sanità Pubblica e Pediatriche, Università degli Studi di Torino, Torino, Italy*

[3] *Dipartimento di Scienze della Vita e Biologia dei Sistemi, Università degli Studi di Torino, Torino, Italy*

[4] *Dipartimento di Oncologia, Università degli Studi di Torino, Torino, Italy*

[5] *Dipartimento di Neuroscienze, Università degli Studi di Torino, Torino, Italy*

§ Equal contribution to the work

* Corresponding authors:

Prof. Roberta Cavalli, Dipartimento di Scienza e Tecnologia del Farmaco, Università degli Studi di Torino, via P. Giuria 9, 10125 Torino, Italy. Phone no.: +39-011-6707686. Fax no.: +39-011-6707687. E-mail address: roberta.cavalli@unito.it

Dr. Giuliana Banche, Dipartimento di Scienze della Sanità Pubblica e Pediatriche, Università degli Studi di Torino, Via Santena 9, 10126 Torino, Italy. Phone no.: +39-011-6705627. Fax no.: +39-011-2365627. E-mail address: giuliana.banche@unito.it

Abstract

Vancomycin (Vm) currently represents the gold standard against methicillin-resistant *Staphylococcus aureus* (MRSA) infections. However, it is associated with low oral bioavailability, formulation stability issues, and severe side effects upon systemic administration. These drawbacks could be overcome by Vm topical administration if properly encapsulated in a nanocarrier. Intriguingly, nanobubbles (NBs) are responsive to physical external stimuli such as ultrasound (US), promoting drug delivery. In this work, perfluoropentane (PFP)-cored NBs were loaded with Vm by coupling to the outer dextran sulfate shell. Vm-loaded NBs (VmLNBs) displayed ~300 nm sizes, anionic surfaces and good drug encapsulation efficiency. *In vitro*, VmLNBs showed prolonged drug release kinetics, not accompanied by cytotoxicity on human keratinocytes. Interestingly, VmLNBs were generally more effective than Vm alone in MRSA killing, with VmLNB antibacterial activity being more sustained over time as a result of prolonged drug release profile. Besides, VmLNBs were not internalized by *staphylococci*, opposite to Vm solution. Further US association promoted drug delivery from VmLNBs through an *in vitro* model of porcine skin. Taken together, these results support the hypothesis that proper Vm encapsulation in US-responsive NBs might be a promising strategy for the topical treatment of MRSA wound infections.

Key words

Nanobubbles; vancomycin; methicillin-resistant *Staphylococcus aureus*; ultrasound; prolonged release.

1. Introduction

Chronic wounds fail to proceed through timely regulated and interrelated processes to restore anatomical and functional integrity of the injured tissues (Lazarus et al., 1994) such as diabetic feet, bedsores, and venous ulcers (Markova et al., 2012). To date, these types of wounds are considered like a silent epidemic, affecting a large fraction of the world population and posing a major gathering threat to the public health and economy of all developed countries (Daeschlein, 2013). Hospitalized patients are at particular risk, especially those suffering from diabetes, human immunodeficiency virus or other immune disorders, as well as those undergoing chemotherapy (Payne et al., 2008).

Beyond delayed healing processes due to different factors (hypoxia, persistent inflammation, and altered balances between tissue remodelling proteinases and their inhibitors), chronic wounds are often worsened by microbial infections (Gurusamy et al., 2013). Among the bacteria responsible for skin infection, *Staphylococcus aureus* represents the most common pathogen to be identified in chronic wounds, with methicillin-resistant *S. aureus* (MRSA) accounting for upward of 20% to 50% of cases (Price, 2010). MRSA colonies often develop at the interface between synthetic prostheses and biological tissues, particularly during surgery and post-surgery course. In addition, MRSA colonization or infection of wounds can result in MRSA bacteremia, which is associated with a 30-day mortality of about 28% to 38% patients (Gurusamy et al., 2013).

The main goal of chronic wound treatment is to decrease the injuring-associated microbial load, thus allowing wound healing processes to take place. However, conventional systemic delivery of antibiotics not only entails poor penetration into ischemic and necrotic tissues, but can also cause systemic toxicity with associated renal and liver complications, resulting in forced hospitalization for further monitoring and advanced treatment. On the contrary, topically applied antimicrobials have proven effective in decreasing bacterial levels in granulating wounds (Diehr et al., 2008). Therefore,

alternative local delivery of antimicrobials - either by topical administration or through novel delivery devices - may enable to keep high local antibiotic concentrations for prolonged release times without reaching systemic toxicity (Zilberman et al., 2008).

A promising approach to develop a topical therapy for microbial infection in skin and soft tissues would employ biocompatible nanomaterials and drug nanocarriers. Indeed, nanotechnology represents an emerging field to be exploited for antibiotic drug delivery. Thanks to their physical and chemical properties (small size, high surface-to-volume ratio and suitable surface modification) nano-sized materials may be used as drug carriers to trespass several physiological barriers and to reach biological targets. The coupling of nanocarriers with anti-infectious agents makes it likely to increase drug concentrations and drug penetration at the site of infection. As a result, it might not only improve the therapeutic index but also reduce some issues associated with nonspecific cytotoxicity and antibiotic resistance (Sharma et al., 2012).

Vancomycin hydrochloride, being effective against many Gram-positive bacteria that are unresponsive to common antibiotics, represents the gold standard against MRSA infections (Kullar et al., 2016). However, Vm is poorly absorbed from the gastrointestinal tract with a low oral bioavailabiliy. Low intravenous infusion is often suggested as a feasible alternative for drug administration, but Vm instability in aqueous solutions at 37°C could imply a tremendous reduction of drug effectiveness (Mawhinney et al., 1992; Raverdy et al., 2013). Following parenteral administration, Vm displays a slow mode of action, a complex concentration-time profile, and a disappointingly low penetration in tissues (Vandecasteele et al., 2012). Furthermore, systemic Vm administration can be associated with several adverse effects (Vidal et al., 1992). On the other hand, Vm topical application – that would be much safer than systemic administration - is currently limited by several factors such as skin barrier properties and poor drug permeability (Giandalia et al., 2001). Being the main goal of chronic wound treatment to decrease the microbial load, allowing the healing processes to take place, new delivery

protocol should be devised, since conventional systemic delivery of antibiotics requires a drug concentration which is locally ineffective because of the poor penetration into ischemic and necrotic tissues, but can cause systemic toxicity and topically applied antimicrobials have proven effective in decreasing bacterial levels in granulating wounds (Diehr et al., 2007), without inducing systemic toxicity (Zilberman et al., 2008) but suffer from poor diffusion across membranes.

Intriguingly, the use of a nanocarrier may help to avoid the abovementioned drawbacks. Notably, nanocarriers such as liposomes, microemulsions, and lipid nanoparticles have the potential to deliver drugs to the skin more efficiently than conventional topical carriers such as creams and ointments, that are not usually recommended for applications on injured skin (Giandalia et al., 2001; Prabhu et al., 2012). However, the response to drug topical applications has been too weak so far, mainly due to the inability to cross the external skin barrier (*stratum corneum*) and reach the dermal regions where the bacteria are nested. Interestingly, physical media such as ultrasound (US) are reportedly able to trigger drug release at the site of infection by temporarily increasing skin permeability through sonophoresis. As such, US is useful to promote drug targeting and transdermal delivery in a non-invasive manner (Azagury et al., 2014; Park et al, 2012).

Microbubbles (MBs) (Guiot et al., 2006), nanobubbles (NBs) (Cavalli et al., 2009a; Cavalli et al., 2009b; Cavalli et al., 2016) and nanodroplets (NDs) (Magnetto et al., 2014; Prato et al., 2015) are suitable carriers to be combined with such a physical trigger. They are spherical core-shell structures filled with gases such as perfluorocarbons. Particularly, oxygen-cored nanostructures can be employed both for sonography (as contrast agents) (Fokong et al., 2012; Marxer et al., 2011) and for therapy (as hypoxia- and infection-counteracting devices) (Gulino et al., 2015; Banche et al., 2015; Khadjavi et al., 2015; Basilico et al., 2015; Prato et al., 2016). In particular NBs, consisting in an outer shell of a biocompatible/biodegradable polysaccharide (chitosan, dextran, or dextran sulfate) and an inner core filled with an oxygen-storing fluorocarbon (perfluoropentane, PFP), have been purposely developed as

a new non-invasive, low-cost and multipurpose nanotechnological platform (Cavalli et al., 2009a; Cavalli et al., 2009b; Cavalli et al., 2016). PFP is a perfluorocarbon with a boiling point of 29°C, hence liquid at room temperature. The use of PFP allows liquid droplet generation at room temperature. Then, PFP in nanodroplets can be activated by an external stimulus, like US, by means of a mechanism called acoustic droplet vaporization, causing the droplet to become a bubble. Depending on the properties of the nanostructure, NBs can be subsequently coupled with different molecules, such as drugs or genetic materials, thus acting as nanocarriers (Cavalli et al., 2012; Cavalli et al., 2013; Delalande et al., 2012; Yin et al., 2014). Due to their structure and their gaseous core, NBs are very responsive to US and can take advantage from a number of effects related to microcavitation and microstreaming, occurring at the liquid-membrane interface and responsible for transitory and reversible openings of the pores, thus crossing the membrane itself and delivering their content beyond the tissue (sonophoresis) or the cell (sonoporation) membrane (Karshafian et al., 2009).

Based on these preconditions, the present work aimed at producing dextran sulfate-shelled and PFP-cored NBs for Vm local delivery to potentially treat skin infectious diseases. The formulation is referred to as “nanobubbles” for sake of simplicity but it must be said that, prior to the application of US, it would be more accurate to use the term “nanodroplets” when the core is constituted of PFP. Therefore, Vm-loaded NBs (VmLNBs) were prepared and characterized for physico-chemical parameters and drug release kinetics; tested for biocompatibility with human skin cells and for their antibacterial properties or interactions with MRSA; and challenged for responsiveness to US, in order to assess their effectiveness as Vm nanocarriers for local delivery.

2. Material and methods

2.1. Materials

All materials were from Sigma-Aldrich, St Louis, MO, unless those indicated as follows. Sterile plastics were from Costar, Cambridge, UK; ethanol (96%) was from Carlo Erba (Milan, Italy); soybean lecithin (Epikuron 200®) was from Cargill (Hamburg, Germany); 1-800 Millipore system to obtain ultrapure water and Amicon® Ultra-0.5 centrifugal filter device were from Millipore (Molsheim, France); Ultra-Turrax SG215 homogenizer was from IKA (Staufen, Germany); RPMI 1640 medium was from Invitrogen (Carlsbad, CA); Nanobrook 90Plus Particle Size Analyzer was from Brookhaven (New York City, NY); Philips CM10 electron microscope was from Philips (Eindhoven, the Netherlands); Ubbelhode capillary viscosimeter was from SCHOTT Instruments GmbH (Mainz, Germany); Perkin Elmer PUMP 250B was from Perkin Elmer (Waltham, MA); Flexar UV/Vis LC spectrophotometer detector was from Perkin Elmer (Waltham, MA); Agilent TC C_{18} columns were from Agilent (Santa Clara, CA); Orion Model 420A pH Meter was from Thermo Scientific (Waltham, MA); Semi-Micro Osmometer K-7400 was from Knauer (Berlin, Germany); Beckman Coulter Allegra 64R Centrifuge was from Beckman Coulter (Brea, CA); Spectra/Por cellulose membranes were from Spectrum Laboratories (Rancho Dominguez, CA); HaCaT cells were from Cell Line Service GmbH (Eppelheim, Germany); cell culture RPMI 1640 and Dulbecco's modified Eagle's medium (DMEM) were from Invitrogen (Carlsbad, CA); streptomycin was from Cambrex Bio Science (Vervies, Belgium); humidified CO_2/air-incubator was from Thermo Fisher Scientific Inc. (Waltham, MA); tryptic soy broth (TSB) and tryptic soy agar (TSA) were from Merk KgaA (Darmstadt, Germany); Olympus Fluoview 200 laser scanning confocal system mounted on an inverted IX70 Olympus microscope was from Olympus America Inc. (Melville, NY, USA) ; SPSS 16.0 software was from SPSS Inc. (Chicago, IL).

2.2. Development and manufacturing of formulations

2.2.1. Determination of Vm and dextran sulfate interaction ratio

Increasing concentrations (0.25, 0.5, 1.0, 2.0 mg/mL) of dextran sulfate aqueous solutions (1 mL) were added to 1 mL of Vm aqueous solution (1 mg/mL) under magnetic stirring at room temperature overnight. After equilibration, the systems were separated by centrifugation (20000 rpm, 15 minutes) using a centrifugal filter device (Amicon® Ultra), in order to determine the amount of unbound Vm in the filtrate phase. The drug concentration in the filtrate was determined using the HPLC method described below.

2.2.2. Preparation of NB, Vm, and VmLNB formulations

NBs were formulated using PFP for the inner core and dextran sulfate for the shell. A purposely tuned multi-step protocol was designed. Briefly, a pre-emulsion was obtained adding 300 μL of an ethanol solution containing Epikuron® 200 and palmitic acid (1% w/v) to 500 μL of PFP under magnetic stirring. After the addition of 4.8 mL of ultrapure water, the system was homogenized using a Ultra-Turrax SG215 homogenizer. To obtain the polymeric NBs, 350 μL of 1% w/v dextran sulfate (molecular weight = 100 kDa) aqueous solution was added drop-wise under magnetic stirring. Blank NBs obtained according to this procedure were employed as control formulations in the subsequent experiments. On the other hand, to obtain VmLNBs, an extra step based on drop-wise addition of a Vm aqueous solution (pH 3.5) to the so-formed NBs was performed under mild stirring. Different concentrations of Vm solutions were added to prepare a series of VmLNB formulations with increasing drug content (0.004, 0.01, 0.1, and 1 mg/mL). VmLNBs were then purified by dialysis to eliminate unbound molecules. For selected experiments, fluorescent NBs and VmLNBs were obtained by the

addition of 6-coumarin (1 mg/mL) to the PFP core. Alternatively, fluorescent Vm was synthesized through reaction between fluorescein isothiocyanate (FITC) and Vm. For this purpose, an amount of FITC solution in methanol (0.2 % w/v) was added to Vm aqueous solution and incubated under stirring overnight in the dark. **Figure 1** shows a representative scheme resuming the general structure of fluorescent VmLNBs. For cell experiments, NBs were prepared in phosphate buffer saline pH 7.4 (PBS). For *in vitro* permeation studies, NBs were prepared in saline solution (NaCl 0.9% w/v).

2.2.3. NB sterilization

Firstly, the glassware and the components were sterilized at 121 °C and 2 bar. Subsequently, all NB formulations were sterilized through UV-C exposure for 20 min. Thereafter, UV-C-treated materials were incubated with cell culture RPMI 1640 medium in a humidified CO_2/air-incubator at 37°C up to 72 h, not displaying any signs of microbial contamination when checked by optical microscopy.

2.3. Characterization of formulations

2.3.1. Characterization of NB and VmLNB formulations

The average diameter, polydispersity index and zeta potential were determined by photocorrelation spectroscopy using a particle size analyzer at a scattering angle of 90° and a temperature of 25 °C. NB suspensions were diluted in deionized filtered water before measurement. For zeta potential determination, samples of diluted NB formulations were placed in the electrophoretic cell, where an electric field of approximately 15 V/cm was applied. The morphology of formulations was evaluated by Transmission Electron Microscopy (TEM), using a Philips CM10 (Eindhoven, NL) instrument. NB and VmLNB aqueous suspensions were sprayed on Formwar-coated copper grid and air-dried before

observation. The viscosity of the samples was determined at 25 °C using a Ubbelhode capillary viscosimeter.

2.3.2. HPLC quantitative Vm determination

Vm quantitative determination was carried out by using an HPLC system based on a Perkin Elmer pump equipped with a spectrophotometer detector. Analyses were performed using an Agilent TC C_{18} column (250 mm × 4.6 mm, 5 µm). The mobile phase was a mixture of KH_2PO_4 50 mM (pH 4) and acetonitrile (92:8 v/v), degassed and pumped through the column with a flow rate of 1 mL/min. Ultraviolet detection was set at 286 nm. The external standard method was used to calculate the drug concentration. For this purpose, 1 mg of Vm was weighted, placed in a volumetric flask, and dissolved in water to obtain a stock standard solution. This solution was then diluted using the mobile phase, providing a series of calibration solutions, subsequently injected into the HPLC system. Linear calibration curve was obtained over the concentration range of 0.5−25 µg/mL, with a regression coefficient of 0.999.

2.3.3. In vitro evaluation of Vm stability

Vm chemical stability - either solved in aqueous solution or loaded in VmLNBs - was evaluated at room temperature and at 37 °C over time. A quantitative determination of Vm concentration over time was carried out using the HPLC method described above.

2.3.4. NB stability over time and after US administration

The physical stability of NBs was evaluated by morphological analysis and by size and zeta potential determination of formulation over time. Their average diameters, zeta potential values and morphology were assessed up to six months. Stability was also investigated following NB exposure to US (f = 2.5±

0.1 MHz; t = 10 min; P = 5 W). NB morphology was observed by TEM to confirm the integrity of NB structure.

2.3.5. Encapsulation efficiency and loading capacity of Vm in NBs

The encapsulation efficiency of VmLNBs was determined using a centrifugal filter system. 150 µL of VmLNB suspension were put in an Amicon® Ultra-0.5 centrifugal filter device and centrifuged at 15000 rpm for 30 minutes using Beckman Coulter Allegra 64R Centrifuge. The solution filtered in the bottom of the tube was quantified and after suitable dilution was analyzed by HPLC, in order to obtain the concentration of free Vm in VmLNBs suspensions. The encapsulation efficiency was calculated by subtracting the amount of free drug from the initial amount of added Vm, according to the following equation:

$$Encapsulation\ efficiency = \frac{(total\ Vm - free\ Vm)}{total\ Vm} \times 100$$

The loading capacity was determined on freeze-dried NB samples. Briefly, a weighted amount of freeze-dried VmLNBs was suspended in 10 mL of water. After sonication and centrifugation, the supernatant was diluted with mobile phase and analyzed by HPLC. The loading capacity of Vm in VmLNBs was calculated as follows:

$$Loading\ capacity = \frac{(total\ Vm - free\ Vm)}{NB\ weight} \times 100$$

2.4. *In vitro* release studies

In vitro drug release experiments were conducted in a multi-compartment rotating cell, comprising a donor chamber separated by a cellulose membrane (cut-off = 12000 Da) from a receiving compartment. One ml of VmLNB suspension at different concentrations (1, 0.1, 0.01 and 0.004 mg/mL) was placed

in the donor chamber. The *in vitro* release kinetics of Vm from VmLNB was compared to a Vm aqueous solution (1 mg/mL) as a control. The receiving phase, containing phosphate buffer 0.05 M (pH 7.4) was withdrawn at regular intervals and replaced with the same amount of fresh buffer. Quantitative determination of Vm in the withdrawn samples was carried out by the HPLC method, as described in the previous paragraph. Data were expressed as % of Vm released over time.

2.5. *In vitro* permeation study

In vitro studies were performed using a vertical diffusion Franz cell to evaluate Vm permeation throughout the skin. The Franz cell consists of a donor compartment, with Vm (1 mg/mL, either free or carried by VmLNBs, $1x10^{12}$ NBs/ml) and a receiving compartment containing 0.9% w/w NaCl saline solution. To simulate the *stratum corneum* properties a membrane pig ear skin was used. Skin slices were isolated with a dermatome from the outer side of pig ears, obtained from a local slaughterhouse, and then were frozen at −18 °C. Before starting the experiments, the skin was equilibrated in NaCl 0.9 % w/w saline solution, in the presence of 0.01% sodium azide to preserve the skin, at 25 °C for 30 min. Then, after washing with saline solution, the skin layer was inserted between the two compartments of the Franz cell, with the stratum corneum side facing towards the donor chamber. The study was carried out for 24 hours and the receiving phase was withdrawn at regular times and replaced with the same amount of fresh receiving medium. The collected samples were then analyzed by HPLC to determine the amount of Vm permeated over time. US abilities to promote Vm permeation were also investigated. For this purpose, a high frequency US transducer (f = 2.5 MHz; P = 5 W; t = 10 min) was combined to a purposely modified vertical diffusion cell. Drug permeation through pig skin after US application was monitored by HPLC analysis of the cumulative amount of antibiotic reaching the receiving phase over time.

2.6. Human biocompatibility studies

2.6.1. Human keratinocyte cell cultures

HaCaT, a long-term cell line of human keratinocytes immortalized from a 62-year old Caucasian male donor (Boukamp et al., 1988), was used for the assessment of Vm and VmLNB biocompatibility. Cells were grown as adherent monolayers in DMEM medium supplemented with 10% fetal bovine serum, 100 U/mL penicillin, 100 µg/mL streptomycin and 2 mM L-glutamine in a humidified CO_2/air-incubator at 37°C. Before starting the experiments, cells were washed with PBS, detached with trypsin/ethylenediaminetetraacetic acid (0.05/0.02 % v/v), washed with fresh medium and plated at a standard density (10^6 cells/well in 6-well plates) in 2 mL of fresh medium.

2.6.2. Vm and VmLNB cytotoxicity

The potential cytotoxic effects of VmLNBs were measured as the release of lactate dehydrogenase (LDH) from HaCaT cells into the extracellular medium. Briefly, cells were incubated in DMEM medium for 24 h with/without 1 mg/mL Vm, either free or carried by VmLNBs, in a humidified CO_2/air-incubator at 37°C. Then, 1 mL of cell supernatants was collected and centrifuged at 12000 rpm for 2 min. Cells were washed with fresh medium, detached with trypsin/ethylenediaminetetraacetic acid (0.05/0.02 % v/v), washed with PBS, resuspended in 1 mL of TRAP (82.3 mM triethanolamine, pH 7.6), and sonicated on ice with a 10 s burst. 5 µL of cell lysates and 50 µL of cell supernatants were diluted with TRAP and supplemented with 0.5 mM sodium pyruvate and 0.25 mM NADH (300 µL as a final volume) to start the reaction. The reaction was followed measuring the absorbance at 340 nm (37 °C) with Synergy HT microplate reader. Both intracellular and extracellular enzyme activities were

expressed as μmol of oxidized NADH/min/well. Finally, cytotoxicity was calculated as the net ratio between extracellular and total (intracellular + extracellular) LDH activities.

2.6.3. Human keratinocyte cell viability

Cell viability was evaluated using 3-(4,5-dimethylthiazol-2-yl)-2,5-diphenyltetrazolium bromide (MTT) assay. HaCaT cells were incubated for 24 h with/without 1 mg/mL Vm, either free or carried by VmLNBs, in a humidified CO_2/air-incubator at 37°C. Thereafter, 20 μL of 5 mg/mL MTT in PBS were added to cells for 3 additional hours at 37 °C. The plates were then centrifuged, the supernatants discarded and the dark blue formazan crystals dissolved using 100 μL of lysis buffer containing 20 % (w/v) sodium dodecyl sulfate, 40 % N,N-dimethylformamide (pH 4.7 in 80 % acetic acid). The plates were then read on Synergy HT microplate reader at a test wavelength of 550 nm and at a reference wavelength of 650 nm.

2.7. Microbiological assays

2.7.1. Determination of vancomycin antimicrobial activity against MRSA

Vm solutions were freshly prepared for each experiment. Determination of the minimum inhibitory concentration (MIC) of vancomycin was carried by the microdilution broth method according to the latest Clinical and Laboratory Standards Institute (CLSI) guidelines (CLSI 2012). Interpretation of the results was performed as outlined in the above mentioned CLSI guidelines (CLSI 2012).

2.7.2. In vitro antibacterial efficiency of VmLNBs against MRSA.

MRSA, isolated from human ulcerated wounds (Infermi Hospital, Biella, Italy), was cultured over night at 37°C in TSB. After incubation, bacteria were re-suspended in 100 mL of TSB, harvested by 10

min centrifugation at 4,000 rpm, diluted in TSB to 10^4 colony-forming-unit (CFU)/mL, as confirmed by colony counts on TSA, and then incubated in TSB with VmLNBs, loaded with Vm at different concentrations (1, 0.1, 0.01, and 0.004 mg/mL), in sterile sampling tubes for 2, 3, 4, 6, and 24 hours at 37°C. Controls represented by either bacteria incubated in TSB, bacteria incubated with blank NBs or bacteria incubated in the presence of free Vm at different concentrations (1, 0.1, 0.01 and 0.004 mg/mL), were also performed. At each incubation time, serial 10-fold dilutions in saline solution (0.9% NaCl) were prepared from each sample, and 100 μL of each dilution were spread on TSA, so that the number of CFU/mL could be determined.

2.7.3. Imaging with confocal laser scanning microscopy

MRSA bacteria were grown in TSB at 37°C in agitation until reaching the concentration of 1x10^^{9} CFU/mL. Then, 1 mL aliquot of bacteria was pelleted (3000g x 10 min at 4°C), resuspended in PBS 1x and incubated with 6-coumarin-labeled VmLNBs, 6-coumarin-labeled NBs, or FITC-labeled Vm at a dilution of 1:11, as for previous experiments performed on eukaryotic cells. Each sample was placed on orbital shaker (160 rpm) in the dark at 37°C for 2h and 4h. After incubation, one drop from each suspension was streaked on poly-L-lysine-coated microscope slides and allowed to dry. Then, bacteria were stained with iodide propidium (PI) in PBS 1X and again allowed to dry. Fluorescence images were taken with an Olympus IX70 inverted laser scanning confocal microscope, and captured using FluoView 200 software.

2.8. Statistical analysis

At least three independent experiments, each one in duplicate or triplicate, were performed for every investigational study. Numerical data are shown as means ± SEM for inferential results or as means ± SD for descriptive results (see Cumming et al., 2007 for an exhaustive review). Imaging data are shown

as representative pictures. All data were analyzed by a one-way Analysis of Variance (ANOVA) followed by Tukey's post-hoc test (software: SPSS 16.0 for Windows, SPSS Inc., Chicago, IL). $P<0.05$ were considered significant.

3. Results

3.1. Characterization of VmLNB and control (blank NB and Vm) formulations

Before NB production, the interaction between dextran sulfate and Vm was firstly investigated to optimize Vm/dextran sulfate ratio. Results indicated that Vm was complexed at 99% by dextran sulfate solution until the concentration of 0.5 mg/mL (data not shown). The Vm/dextran sulfate ratio was calculated corresponding to 2:1 (w/w). Based on this preliminary information, NBs were prepared according to the protocol described in the Materials and Methods section. After manufacturing, VmLNB and blank NB formulations (with or without 6-coumarin in the inner core) were characterized physico-chemically. Results are shown in **Figure 2** and **Table 1**. Both VmLNBs and NBs displayed spherical shapes with a core-shell structure by TEM analyses. All sizes were in the nanometer range, with all formulations displaying around 300 nm as a value for average diameters. All polidispersity indexes were included between 0.22 and 0.25. Zeta potentials ranged from -34 mV (NBs) to -29 mV (VmLNBs). The loading of Vm in the NB structure did not significantly affect the viscosity of the formulations. NBs were able to load Vm with an encapsulation efficiency of 86% and loading capacity of 29%.

3.2. Stability of VmLNB and control (blank NB and Vm) formulations

NB and VmLNB formulations proved to be physically stable over time, as confirmed by long-term checking of the parameters assessed in the previous paragraph. Indeed, the obtained values did not remarkably change up to six months after the manufacturing of the formulations stored at 4 °C (data not shown). Furthermore, the chemical stability of the drug was comparatively checked between free Vm solution and VmLNB aqueous suspension either over time (up to 14 days) or at different temperatures (25°C and 37°C). As shown in **Figure 3**, the drug resulted much more stable from a

chemical point of view when properly incorporated in the nanocarrier (VmLNBs) than as such in solution.

3.3. Human biocompatibility

The potential toxicity of Vm solution and VmLNB suspension on human skin cells was assessed by testing *in vitro* cultured HaCaT keratinocytes. Cells were incubated for 24 h alone, with 10% v/v Vm solution, or with VmLNB nanosuspensions in normoxic conditions (20% O_2). Thereafter, cytotoxicity was analyzed by LDH assay, and cell viability by MTT assay. As shown in **Figure 4**, neither Vm nor VmLNBs did show significant toxic effects and HaCaT cell viability was not significantly affected by either formulation.

3.4. *In vitro* drug release from VmLNBs

In vitro drug release from VmLNB nanosuspension and free Vm solution were comparatively evaluated over time. As shown in **Figure 5** (time course studies up to 6 h) and **Table 2** (end-point data up to 24 h), 1 mg/mL Vm release from VmLNBs was slow and prolonged over time, compared to free drug solution diffusion. No initial burst effect was observed indicating Vm incorporation in NB shell. Further information on additional incubation times and drug concentrations for VmLNBs is available in Supplementary Materials (**Table S3**). Vm/VmLNB drug release ratios at different times (2, 3, 4, 6, and 24 h) were also calculated (see **Table 2**), in order to allow normalization of the results from treatment with VmLNBs in the microbiological experiments described in the following paragraph.

3.5. *In vitro* antimicrobial activity of VmLNBs

According to preliminary microbiological analyses performed on the MRSA strain employed in the present experiments, 0.004 mg/mL resulted as the MIC value for Vm. Therefore, decreasing Vm concentrations from 1 mg/mL (used for the studies described in the previous paragraphs) to 0.004 mg/mL (MIC value) were employed in a series of experiments aimed at comparatively evaluating Vm (either free or carried by VmLNBs) antibacterial effectiveness against MRSA. Bacteria were incubated at different times (2, 3, 4, 6, and 24 h) either alone (ctr) or with free Vm, VmLNBs, or blank NBs. The initial drug concentrations (1; 0.1; 0.01; and 0.004 mg/mL) loaded on VmLNBs were the same as those solved in free Vm solution. However, as emerged in the previous paragraph, drug release from VmLNBs is significantly slower than free Vm solution diffusion. For this reason, before proceeding with the analysis of the results, all values on bacterial growth referring to Vm- and VmLNB-treated samples were normalized upon time-dependent Vm/VmLNB drug release ratios shown in **Table 2**. Normalized results are shown in **Figure 6**, whereas raw data are available in Supplementary Materials (**Figure S2**). 1 mg/mL Vm effectively inhibited bacterial growth at all times, independently from being free or carried by the nanocarrier. Lower drug concentrations of free Vm solution were effective against MRSA only after longer times of incubation (at least 3 h for 0.1 mg/mL and 0.01 mg/mL Vm; and at least 4 h for 0.004 mg/mL Vm). Interestingly, Vm antibacterial efficacy was significantly improved when the drug was carried by VmLNBs. Indeed, VmLNB-dependent inhibition of bacterial growth was significantly enhanced compared to free Vm solution, at all drug concentrations. Additionally, compared to free Vm solution, VmLNB antibacterial effects appeared earlier, as they were already evident after 2 h of incubation (the first time-point of the observational period) at all Vm concentrations. Blank NBs did not show any antibacterial activity.

Further analysis by confocal microscopy (**Figure 7**) displayed that MRSA avidly internalized free fluorescent Vm already after 2 h of incubation, but not fluorescent VmLNBs. Fluorescent Vm-free NBs did adhere to the bacterial cell wall without being internalized.

3.6. US-triggered drug permeation

The ability of US to promote Vm permeation through the skin was assayed by employing a purposely modified Franz cell constituted by a donor and a recipient chamber separated by a pig skin layer (see **Figure 8A** for a schematic representation of the apparatus). As shown in **Figure 8B**, the administration of US (t = 10 min; f = 2.5 MHz; P = 5 W) strongly induced VmLNBs to deliver the antibiotic drug from the donor chamber throughout the pig skin membrane into the recipient chamber up to 6 h. Furthermore, drug accumulated in the skin after US treatment reached 158 $\mu g/cm^2$ after 6 hours.

4. Discussion

Vm currently represents the main stay against MRSA infections (Koyama et al., 2013; Kullar et al., 2016). However, Vm administration raises several issues that urgently need to be faced, including its marked instability, low oral bioavailability, complex concentration-time profile, low tissue penetration (ranging from 10% in diabetic to 30% in normal skin and soft tissues), and several adverse effects (Mawhinney et al., 1992; Raverdy et al., 2013; Vandecasteele et al., 2012; Vidal et al., 1992; Giandalia et al., 2001). In the attempt to counteract these drawbacks, thus improving the effectiveness of Vm delivery, some novel nanocarriers have been developed: i) Vm coupling to chitosan as an ocular drug delivery vehicle for topical use in rabbit eyes has appeared more effective than carrier-free Vm (Khangtragool et al., 2011); ii) PEGylated liposomal Vm enhanced the effective treatment of MRSA pneumonia and simultaneously reduced the nephrotoxicity risk compared with conventional and non-PEGylated Vm formulations (Muppidi et al., 2011); iii) Vm-loaded liposomes, stabilized with chitosan modified gold nanoparticles bounded to their surface, have proven effective in inhibiting the bacterial growth (Pornpattananangkul et al., 2011); and iv) Vm-containing trehalose and hydroxyethylcellulose spherical matrices have been developed as new delivery systems suitable for topical applications on extensive and purulent wounds (Giandalia et al., 2001). Recently, Vm-loaded polymersosomes were developed from a novel pegylated oleic acid polymer for sustained antibiotic delivery (Omolo et al., 2017). Overall, these works represent the proof-of-principle for the feasibility of choice of nanocarriers, as alternative drug delivery systems to obtain the desired drug release rates and bioavailability (Kalhapure et al., 2015). However, the effectiveness of those nanocarriers was seriously undermined by their poor ability to cross the *stratum corneum*, a skin barrier displaying low permeability unless proper exogenous physical stimuli are provided (Azagury et al., 2014; Park et al, 2012).

For these reasons, the present study aimed at developing Vm nanocarriers as a new platform to be effectively and safely employed for Vm topical administration to treat wound infections. To this purpose, NBs with core-shell nanostructures were identified as first choice carriers due to their known benefits in association with drug delivery, including small size, stability, suitability for drug loading, responsiveness to external stimuli such as US, and controlled drug release abilities (Marano et al., 2016; Cavalli et al., 2009a; Cavalli et al., 2009b; Cavalli et al., 2016). In this study, dextran sulfate was chosen as main constituent of the polysaccharidic shell as a consequence of the large amount of data from the literature supporting dextran biocompatibility (Bos et al., 2005; De Groot et al., 2001). Encouragingly, dextran-based hydrogels have already been employed as matrices in tissue engineering, without showing signs of inflammation *in vivo* (Möller et al., 2007), and recent toxicological studies have shown that dextran, as well as the products from its mechano-chemical processing, can be classified as class 4 (low-toxicity) substances (Dushkin et al., 2013). Moreover, dextran sulfate presents a negative charge that can electrostatically interact with the positive charged Vm. On the other hand, PFP was employed as principal constituent of the inner core, since it is the most widely used fluorocarbon in oxygenating emulsions and NB formulations (Cabrales and Intaglietta, 2013, Castro and Briceno, 2010). In order to load Vm, dextran sulfate-shelled/PFP-cored NBs were then functionalized by exploiting the electrostatic interactions occurring between the negatively charged sulfate groups of the shell and the protonated amino groups of the drug. The obtained VmLNBs displayed a spherical shape and a well-defined core-shell structure with a polymeric shell thickness of about 40 nm, average diameters of 300 nm, viscosity of 1.25 cP, and negatively charged surfaces. Of note, the observed decrease of zeta potential values of ~ 15 % for VmLNBs (around -29 mV) with respect to blank NBs (around -34 mV) confirmed the occurrence of electrostatic interactions between positive amino groups of the drug and negative sulfate groups of the polymer, leading to a partial

charge neutralization of the bubble surface and allowing a good Vm encapsulation efficiency (86%) and loading capacity (29%) in the NB systems.

In addition, it should be noticed that since the zeta potential measures charge repulsion or attraction between particles, it represents a fundamental parameter to avoid nanoparticle aggregation, with zeta potentials lower than -25 mV or larger than +25 mV being generally required for physical stability of colloid systems (Shah and Eldridge, 2014). The stability of VmLNB formulations was further confirmed by long-term checking of their size, surface charge, and viscosity values, which did not show any significant changes up to six months after manufacturing, stored at 4 °C. On the other hand, drug stability was comparatively checked between free Vm solution and VmLNB suspension either over time (up to 14 days) or at different temperatures (25°C and 37°C), revealing an increased stability for Vm when properly encapsulated in the nanocarriers. This appears as an undoubtedly advantageous feature for VmLNB formulations, since they might prove useful to overcome the reported instability of Vm in aqueous solutions at body temperature (Mawhinney et al., 1992, Raverdy et al., 2013). Interestingly, VmLNBs displayed a slow and prolonged drug release kinetics compared to Vm aqueous solution, with only 16% of the drug being released from VmLNBs after 6 h. These data support the hypothesis that VmLNBs may be employed as an effective drug reservoir until reaching the target site, where the antibiotic would be released upon sonication at an appropriate moment only. The features of VmLNBs might be exploited for the design of innovative wound dressing following their inclusion in polymeric base. Indeed, NBs can be dispersed in polymer gel without changing physico-chemical characteristics, as previously showed (Prato et al., 2015). Another intriguing feature of VmLNBs relies on the reported evidence that surface charges play a pivotal role in making a nanoparticle suitable for topical treatment, since they enhance its interaction with the skin and improve its therapeutic effect on inflamed cutaneous tissues, either without (Abdel-Mottaleb et al., 2012) or with concomitant US treatment (Lopez et al., 2011). Although cationic nanoparticles are generally preferred for topical

508 treatment due to the anionic nature of the skin (Wu et al., 2010), some authors have shown that anionic
509 nanoparticles can be more effective (Lee et al., 2013) and less toxic (Ryman-Rasmussen et al., 2007)
510 than the cationic ones. These latter data appear consistent with our results through investigation by
511 biochemical assays to assess VmLNB biocompatibility with human skin tissues. Indeed, VmLNBs did
512 not induce any *in vitro* cytotoxic effects on HaCaT keratinocytes, a skin cell line that was originally
513 immortalized from a 62-year old donor (Boukamp et al., 1988). This peculiar information strengthens
514 remarkably the evidence on VmLNB safety for future topical applications.
515 VmLNB and carrier-free Vm antimicrobial activity against MRSA were comparatively investigated,
516 also analyzing Vm and NB physical interaction with the bacterial cell wall by confocal microscopy.
517 Interestingly, VmLNBs were more effective in MRSA bacterial growth inhibition then free Vm,
518 promoting enhanced and earlier antibacterial effects, although they were not internalized by bacteria,
519 opposite to free Vm. This behavior appears to be a likely consequence of time-sustained release of Vm
520 from VmLNBs.
521 Notably, an important issue that requires caution while evaluating the feasibility for any topical drug
522 treatment is represented by the considerably low degree of permeability of the skin, the primary
523 defense system for the body. This organ consists of several layers, including the *stratum corneum*, the
524 epidermis, and the dermis. In particular the *stratum corneum* - composed of corneocytes interspersed in
525 a laminate of compressed keratin and intercorneocyte lipid lamellae - is very poorly permeable to
526 foreign molecules and represents the main obstacle to transdermal drug delivery (Naik et al., 2000).
527 However, an ideal antibiotic drug formulation should be efficiently localized in the epidermis/dermis
528 and provide a sustained drug release over time (Prabhu et al., 2012). To allow a drug to penetrate the
529 skin, several approaches have been proposed, including skin patches, ionophoresis, chemical
530 enhancers, and US-triggered sonophoresis (Park et al., 2014).

Interestingly, antimicrobial properties have been reported for US, although its effectiveness strongly varies depending on the targeted type of pathogen (fungi vs bacteria; cocci vs bacilli; Gram-positive vs Gram-negative) (Sango et al., 2014). Furthermore, synergistic effects between US and antibiotics have been reported in a series of studies: i) antibiotic treatment coupled with US irradiation resulted in enhanced bactericidal activity against both Gram-positive and Gram-negative bacteria, especially for aminoglycosides (Yu et al., 2012); ii) the combination of Vm and US decreased *S. aureus* viable counts by two orders of magnitude compared to Vm alone (Ayan et al., 2008); and iii) the addition of NB-enhanced US to doxycycline treatment improved the drug effectiveness in eradicating intracellular *Chlamydia trachomatis* (Ikeka-Dantsuji et al., 2011). US-dependent enhancement of antibiotic action on biofilms was named as a 'bioacoustic effect'. Interestingly, Vm transfer through *S. epidermidis* biofilms was shown to be significantly enhanced by US, with bubbles being able to increase the biofilm permeability to Vm (Dong et al., 2013).

As discussed previously, VmLNBs can be effectively employed as an important reservoir to store the drug until trespassing the *stratum corneum* of the skin and reaching the target site. In order to achieve the latter goal, US was assayed for its ability to induce VmLNBs to trespass an *in vitro* cutaneous layer, thereby releasing Vm throughout the skin. Notably, the skin from the pig ear is widely recognized as a good model for human skin permeability, since it displays human-like histological and physiological properties, including epidermal thickness and composition, dermal structure, lipid content and general morphology (Dick and Scott, 1992). The validity of the porcine model has been established by comparing the permeability of simple marker molecules with the corresponding values across human skin (Herkenne et al., 2006, Sekkat et al., 2002). Therefore, the porcine ear skin represents so far the most accountable *in vitro* model to mimic the human skin in studies on percutaneous penetration (Jacobi et al., 2007). In our experiments, US appeared essential to promote Vm release from VmLNBs throughout the pig skin layers, in line with previous reports on NBs and sonophoresis. On the contrary,

the passive transport of free vancomycin hydrochloride was negligible, being a charged and hydrophilic molecule. The amount of Vm accumulated in the skin after US application combined with NBs was greater than MIC value.

5. Conclusions

In the present work, dextran sulfate-shelled and PFP-filled NBs were developed for Vm delivery. VLNBs proved to be effective in MRSA bacterial killing without showing toxic effects on human keratinocytes. The combination of NBs and US enhanced Vm permeation through pig skin and promoted drug skin accumulation. Based on these results, Vm topical administration through proper NB formulations might be a promising strategy for the local treatment of MRSA skin infections. The study represents the proof of concept for the future development of advanced multifunctional therapeutic systems to treat infected wounds.

Acknowledgements

The present work was supported by funds from University of Torino (ex 60% to RC and RS), Compagnia di San Paolo (ORTO11CE8R 2011 to CG and Torino_call2014_L2_207 to AMC), and Fondazione Cariplo (HyWonNa project grant to MP). Thanks are due to Aurelio Malabaila for providing MRSA strain and to Giorgio Gribaudo for allowing to use his lab facilities to perform confocal microscopy studies.

References

Abdel-Mottaleb, M.M., Moulari, B., Beduneau, A., Pellequer, Y., Lamprecht, A., 2012. Surface-charge-dependent nanoparticles accumulation in inflamed skin. J. Pharm. Sci.101, 4231-4239.

Ayan, İ., Aslan, G., Çömelekoğlu, Ü., Yılmaz, N., Çolak, M., 2008. The effect of low-intensity pulsed sound waves delivered by the Exogen device on Staphylococcus aureus morphology and genetics. Acta orthop. traumatol. turc. 42(4), 272-277.

Azagury, A., Khoury, L., Enden, G., Kost, J., 2014. Ultrasound mediated transdermal drug delivery. Adv. drug del. rev. 72, 127-143.

Banche, G., Prato, M., Magnetto, C., Allizond, V., Giribaldi, G., Argenziano, M., Khadjavi, A., Gulino, G.R., Finesso, N., Mandras, N., Tullio, V., Cavalli, R., Guiot, C., Cuffini, A.M., 2015. Antimicrobial chitosan nanodroplets: new insights for ultrasound-mediated adjuvant treatment of skin infection. Future Microbiol. 10(6), 929-939. doi: 10.2217/fmb.15.27. PubMed PMID: 26059617.

Basilico, N., Magnetto, C., D'Alessandro, S., Panariti, A., Rivolta, I., Genova, T., Khadjavi, A., Gulino, G.R., Argenziano, M., Soster, M., Cavalli, R., Giribaldi, G., Guiot, C., Prato, M., 2015. Dextran-shelled oxygen-loaded nanodroplets reestablish a normoxia-like pro-angiogenic phenotype and behavior in hypoxic human dermal microvascular endothelium. Toxicol. Appl. Pharmacol. 288(3), 330-338. doi: 10.1016/j.taap.2015.08.005. Epub 2015 Aug 12. PubMed PMID: 26276311.

Bos, G.W., Hennink, W.E., Brouwer, L.A., den Otter, W., Veldhius, F.J., van Nostrum, C.F., van Luyn M.J., 2005. Tissue reactions of in situ formed dextran hydrogels crosslinked by stereocomplex formation after subcutaneous implantation in rats. Biomaterials 26, 3901–3909.

Boukamp, P., Dzarlieva-Petrusevska, R.T., Breitkreuz, D., Hornung, J., Markham, A., Fusenig, N.E., 1988. Normal keratinization in a spontaneously immortalized aneuploid human keratinocyte cell line. J. Cell. Biol. 106, 761-771.

Cabrales, P., Intaglietta, M., 2013. Blood substitutes: evolution from noncarrying to oxygen- and gas-carrying fluids. ASAIO J. 59, 337-354.

Castro, C.I., Briceno, J.C., 2010. Perfluorocarbon-based oxygen carriers: review of products and trials. Artif. Organs. 34, 622-634.

Cavalli, R., Bisazza, A., Rolfo, A., Balbis, S., Madonnaripa, D., Caniggia, I., Guiot, C., 2009a. Ultrasound-mediated oxygen delivery from chitosan nanobubbles. Int. J. Pharm. 378, 215–217.

Cavalli, R., Bisazza, A., Giustetto, P., Civra, A., Lembo, D., Trotta, G., Guiot, C., Trotta, M., 2009b. Preparation and characterization of dextran nanobubbles for oxygen delivery. Int. J. Pharm. 381, 160-165.

Cavalli, R., Bisazza, A., Trotta, M., Argenziano, M., Civra, A., Donalisio, M., Lembo, D., 2012. New chitosan nanobubbles for ultrasound-mediated gene delivery: preparation and in vitro characterization. Int. J. Nanomed. 7, 3309-3318.

624 Cavalli, R., Bisazza, A., Lembo, D., 2013. Micro-and nanobubbles: A versatile non-viral platform for
625 gene delivery. Int. J. Pharm. 456(2), 437-445.
626
627 Cavalli, R., Soster, M., Argenziano, M., 2016. Nanobubbles: a promising efficienft tool for therapeutic
628 delivery. Ther. Deliv. 7(2), 117-138. doi: 10.4155/tde.15.92. Epub 2016 Jan 15. PubMed PMID:
629 26769397.
630
631 Clinical and Laboratory Standards Institute. Performance standards for antimicrobial susceptibility
632 testing. Twenty-second informational supplement. Document M100-S22. Vol . 32, No. 3. Wayne, PA:
633 CLSI; 2012.
634
635 Cumming, G., Fidler, F., Vaux, D.L., 2007. Error bars in experimental biology. J Cell Biol. 177, 7-11.
636
637 Daeschlein, G., 2013. Antimicrobial and antiseptic strategies in wound management. Int. Wound J.
638 10(1), 9-14. doi: 10.1111/iwj.12175. Review. PubMed PMID:24251838.
639
640 De Groot C.J., Van Luyn, M.J.A., Van DijK-Wolthuis, Cadée, J.A., Plantinga, J.A., Den Otter, W.,
641 Hennink, W.E., 2001. In vitro biocompatibility of biodegradable dextran-based hydrogels tested with
642 human fibroblast. Biomaterials 22, 1197–1203.
643
644 Delalande, A., Postema, M., Mignet, N., Midoux, P., Pichon, C., 2012. Ultrasound and microbubble-
645 assisted gene delivery: recent advances and ongoing challenges. Ther. Deliv. 3, 1199-1215.
646

Dick, I.P., Scott, R.C. 1992. Pig ear skin as an in-vitro model for human skin permeability. J. Pharm. Pharmacol. 44, 640–645.

Diehr, P., O'Meara, E.S., Fitzpatrick, A., Newman, A.B., Kuller, L., Burke, G., 2008. Weight, mortality, years of healthy life, and active life expectancy in older adults. J. Am. Geriatr. Soc. 56(1), 76-83. Epub 2007 Nov 20. PubMed PMID: 18031486; PubMed Central PMCID: PMC3865852.

Dong, Y., Chen, S., Wang, Z., Peng, N., Yu, J., 2013. Synergy of ultrasound microbubbles and vancomycin against Staphylococcus epidermidis biofilm. J. Antimicrob. Chemother. 68, 816-826.

Dushkin, A.V., Meteleva, E.S., Tolstikova, T.G., Pavlova, A.V., Khvostov, M.V. 2013. Gel chromatographic and toxicological studies of the mechanochemical transformations of water-soluble polysaccharides. Pharm. Chem. J. 46, 630-633.

Fokong, S., Theek, B., Wu, Z., Koczera, P., Appold, L., Jorge, S., Resch-Genger, U., VanZandvoort, M., Storm, G., Kiessling, F., Lammers, T., 2012. Image-guided, targeted and triggered drug delivery to tumors using polymer-based microbubbles. J. Control. Rel. 163, 75–81.

Giandalia, G., De Caro, V., Cordone, L., Giannola, L.I. 2001. Trehalose-hydroxyethylcellulose microspheres containing vancomycin for topical drug delivery. Eur. J. Pharm. and Biopharm.: official journal of Arbeitsgemeinschaft fur Pharmazeutische Verfahrenstechnik e.V. 52, 83-89.

669 Guiot, C., Pastore, G., Napoleone, M., Gabriele, P., Trotta, M., Cavalli, R., 2006. Thermal response of
670 contrast agent microbubbles: preliminary results from physico-chemical and US-imaging
671 characterization. Ultrasonics. 44(1), 127-130. Epub 2006 Jun 30. PubMed PMID: 17056082.
672
673 Gulino, G.R., Magnetto, C., Khadjavi, A., Panariti, A., Rivolta, I., Soster, M., Argenziano, M., Cavalli,
674 R., Giribaldi, G., Guiot, C., Prato, M., 2015. Oxygen-Loaded Nanodroplets Effectively Abrogate
675 Hypoxia Dysregulating Effects on Secretion of MMP-9 and TIMP-1 by Human Monocytes. Mediators
676 Inflamm. 2015, 964838. doi: 10.1155/2015/964838. Epub 2015 Mar 23. PubMed PMID: 25878404;
677 PubMed Central PMCID: PMC4386605.
678
679 Gurusamy, K.S., Koti, R., Toon, C.D., Wilson, P., Davidson, B.R., 2013. Antibiotic therapy for the
680 treatment of methicillin-resistant Staphylococcus aureus (MRSA) infections in surgical wounds.
681 Cochrane Database Syst. Rev. 20, 8:CD009726. doi: 10.1002/14651858.CD009726.pub2. Review.
682 PubMed PMID: 23963687.
683
684 Herkenne, C., Naik, A., Kalia, Y.N., Hadgraft, J., Guy, R.H., 2006. Pig ear skin ex vivo as a
685 model for in vivo dermatopharmacokinetic studies in man. Pharm. Res. 23, 1850-1856.
686
687 Ikeda-Dantsuji, Y., Feril, L. B., Tachibana, K., Ogawa, K., Endo, H., Harada, Y., Suzuki, R.,
688 Maruyama, K., 2011. Synergistic effect of ultrasound and antibiotics against Chlamydia trachomatis-
689 infected human epithelial cells in vitro. Ultrason. sonochem. 18(1), 425-430.
690
691 Jacobi, U., Kaiser, M., Toll, R., Mangelsdorf, S., Audring, H., Otberg, N., Sterry, W., Lademann, J.,
692 2007. Porcine ear skin: an in vitro model for human skin. Skin Research and Technology 13(1), 19–24.

693 Karshafian, R., Bevan, P.D., Williams, R., Samac, S., Burns, P.N., 2009. Sonoporation by ultrasound-
694 activated microbubble contrast agents: effect of acoustic exposure parameters on cell membrane
695 permeability and cell viability. Ultrasound Med. Biol. 35, 847-860.
696
697 Khadjavi, A., Magnetto, C., Panariti, A., Argenziano, M., Gulino, G.R., Rivolta, I., Cavalli, R.,
698 Giribaldi, G., Guiot, C., Prato, M., 2015. Chitosan-shelled oxygen-loaded nanodroplets abrogate
699 hypoxia dysregulation of human keratinocyte gelatinases and inhibitors: New insights for chronic
700 wound healing. Toxicol. Appl. Pharmacol. 286(3), 198-206. doi: 10.1016/j.taap.2015.04.015. Epub
701 2015 Apr 30. PubMed PMID: 25937238.
702
703 Kalhapure, R.S., Suleman, N., Mocktar, C., Seedat, N., Govender, T., 2015. Nanoengineered Drug
704 Delivery Systems for Enhancing Antibiotic Therapy. J. Pharm. Sci. 104, 872–905.
705
706 Khangtragool, A., Ausayakhun, S., Leesawat, P., Laokul, C., Molloy, R., 2011. Chitosan as an ocular
707 drug delivery vehicle for vancomycin. J. App. Pol. Sci. 122, 3160-3167.
708
709 Koyama, N., Inokoshi, J., Tomoda, H., 2012. Anti-infectious agents against MRSA. Molecules 18(1),
710 204-224. doi: 10.3390/molecules18010204.
711
712 Kullar, R., Sakoulas, G., Deresinski, S., van Hal, S. J., 2016. When sepsis persists: a review of MRSA
713 bacteraemia salvage therapy. J. Antimicrob. Chemother. 71, 576-586.
714

Lazarus, G.S., Cooper, D.M., Knighton, D.R., Percoraro, R.E., Rodeheaver, G., Robson, M.C., 1994. Definitions and guidelines for assessment of wounds and evaluation of healing. Wound Repair Regen. 2(3), 165-170. PubMed PMID: 17156107.

Lee, O., Jeong, S.H., Shin, W.U., Lee, G., Oh, C., Son, S.W., 2013. Influence of surface charge of gold nanorods on skin penetration. Skin Res. Technol. 19, e390-e396.

Lopez, R.F., Seto, J.E., Blankschtein, D., Langer, R., 2011. Enhancing the transdermal delivery of rigid nanoparticles using the simultaneous application of ultrasound and sodium lauryl sulfate. Biomaterials. 32, 933-941.

Magnetto, C., Prato, M., Khadjavi, A., Giribaldi, G., Fenoglio, I., Jose, J., Gulino, G.R., Cavallo, F., Quaglino, E., Benintende, E., Varetto, G., Troia, A., Cavalli, R., Guiot, C., 2014. Ultrasound-activated decafluoropentane-cored and chitosan-shelled nanodroplets for oxygen delivery to hypoxic cutaneous tissues. RSC Advances 4, 38433-38441.

Marano, F., Argenziano, M., Frairia, R., Adamini, A., Bosco, O., Rinella, L., Fortunati, N., Cavalli, R., Catalano, M.G., 2016. Doxorubicin-Loaded Nanobubbles Combined with Extracorporeal Shock Waves: Basis for a New Drug Delivery Tool in Anaplastic Thyroid Cancer. Thyroid 26(5), 705-716

Markova. A., Mostow, E.N., 2012. US skin disease assessment: ulcer and wound care. Dermatol. Clin. 30(1), 107-111. ix. doi: 10.1016/j.det.2011.08.005. Review. PubMed PMID: 22117872.

738 Marxer, E.E.J., Brüßler, J., Becker, A., Schümmelfeder, J., Schubert, R., Nimsky, C., Bakowsky, U.,
739 2011. Development and characterization of new nanoscaled ultrasound active lipid dispersions as
740 contrast agents. Eur. J. Pharm. Biopharm. 77, 430–437.
741
742 Mawhinney, W.M., Adair, C.G., Gorman, S.P., McClurg, B., 1992. Stability of vancomycin
743 hydrochloride in peritoneal dialysis solution. Am. J. Hosp. Pharm. 49(1), 137-139. PubMed PMID:
744 1570857.
745
746 Möller, S., Weisser, J., Bischoff, S., Schnabelrauch, M., 2007. Dextran and hyaluronan methacrilate
747 based hydrogels as matrices for soft tissue reconstruction. Biomol. Eng. 24, 496–504.
748
749 Muppidi, K., Wang, J., Betageri, G., Pumerantz, A.S. 2011. PEGylated liposome encapsulation
750 increases the lung tissue concentration of vancomycin. Antimicrob. Agents Chemother. 55(10), 4537-
751 4542.
752
753 Naik, A., Kalia, Y.N., Guy, R.H., 2000. Transdermal drug delivery: overcoming the skin's barrier
754 function. Pharm. Sci. Technol. Today. 3, 318–326.
755
756 Omolo, C.A., Kalhapure, R.S., Jadhav, M., Rambharose, S., Mocktar, C., Ndesendo, V.M., Govender,
757 T. 2017. PEGylated oleic acid: A promising amphiphilic polymer for nano-antibiotic delivery. Eur. J.
758 Pharm. Biopharm. 112, 96-108.
759

760 Park, D., Ryu, H., Kim, H.S., Kim, Y.S., Choi, K.S., Park, H., Seo J., 2012. Sonophoresis Using
761 Ultrasound Contrast Agents for Transdermal Drug Delivery: An In Vivo Experimental Study.
762 Ultrasound Med. & Biol. 38(4), 642-650.
763
764 Park, D., Park, H., Seo, J., Lee, S., 2014. Sonophoresis in transdermal drug delivery. Ultrasonics. 54,
765 56-65.
766
767 Payne, W.G., Naidu, D.K., Wheeler, C.K., Barkoe, D., Mentis, M., Salas, R.E., Smith, D.J., Robson,
768 M.C., 2008. Wound healing in patients with cancer. Eplasty. 8, e9. PubMed PMID: 18264518; PubMed
769 Central PMCID: PMC2206003.
770
771 Pornpattananangkul, D., Zhang, L., Olson, S., Aryal, S., Obonyo, M., Vecchio, K., Huang, C.M.,
772 Zhang, L., 2011. Bacterial toxin-triggered drug release from gold nanoparticle-stabilized liposomes for
773 the treatment of bacterial infection. J. American Chem. Soc.133(11), 4132-4139.
774
775 Prabhu, P., Patravale, V., Joshi, M., 2012. Nanocarriers for effective topical delivery of anti-infectives.
776 Current Nanoscience 8, 491-503.
777
778 Prato, M., Magnetto, C., Jose, J., Khadjavi, A., Cavallo, F., Quaglino, E., Panariti, A., Rivolta, I.,
779 Benintende, E., Varetto, G., Argenziano, M., Troia, A., Cavalli, R., Guiot C., 2015. 2H,3H-
780 decafluoropentane-based nanodroplets: new perspectives for oxygen delivery to hypoxic cutaneous
781 tissues. Plos One 10(3), e0119769. doi:10.1371/journal.pone.0119769
782

Prato, M., Khadjavi, A., Magnetto, C., Gulino, G.R., Rolfo, A., Todros, T., Cavalli, R., Guiot, C., 2016. Effects of oxygen tension and dextran-shelled/2H,3H-decafluoropentane-cored oxygen-loaded nanodroplets on secretion of gelatinases and their inhibitors in term human placenta. Biosci Biotechnol Biochem. 80(3), 466-472. doi: 10.1080/09168451.2015.1095068. Epub 2015 Nov 2. PubMed PMID: 26523859.

Price, M., 2010. Community-acquired methicillin-resistant Staphylococcus aureus: an ongoing challenge for WOC nursing. J Wound Ostomy Continence Nurs. 37(6), 633-638. doi: 10.1097/WON.0b013e3181feb001. Review. PubMed PMID: 21076263.

Raverdy V., Ampe, E., Hecq, J.D., Tulkens, P. M., 2013. Stability and compatibility of vancomycin for administration by continuous infusion. J. Antimicrob. Chemother. 68, 1179-1182.

Ryman-Rasmussen, J.P., Riviere, J.E., Monteiro-Riviere, N.A., 2007. Surface coatings determine cytotoxicity and irritation potential of quantum dot nanoparticles in epidermal keratinocytes. J Invest Dermatol. 127, 143-153.

Sango, D.M., Abela, D., McElhatton, A., Valdramidis, V.P., 2014. Assisted ultrasound applications for the production of safe foods. J. Appl. Microbiol. 116, 1067-1083.

Sekkat, N., Kalia, Y.N., Guy, R.H., 2002. Biophysical study of porcine ear skin in vitro and its comparison to human skin in vivo. J. Pharm. Sci. 91, 2376-2381.

Shah, R., Eldridge, R., 2014. Optimisation and Stability Assessment of Solid Lipid Nanoparticles using Particle Size and Zeta Potential. J. Phys. Sci, 25, 59–75

807 Sharma, A., Arya, D.K., Dua, M., Chhatwal, G.S., Johri, A.K., 2012. Nano-technology for targeted
808 drug delivery to combat antibiotic resistance. Expert Opinion Drug Del. 9, 1325-1332.
809
810 Vandecasteele, S.J., De Vriese, A.S., Tacconelli, E., 2012. The pharmacokinetics and
811 pharmacodynamics of vancomycin in clinical practice: evidence and uncertainties. J. Antim. Chem. 68,
812 743-748.
813
814 Vidal, C., González Quintela, A., Fuente, R., 1992. Toxic epidermal necrolysis due to vancomycin.
815 Ann Allergy. 68(4), 345-347. PubMed PMID: 1558331.
816
817 Wu, X., Landfester, K., Musyanovych, A., Guy, R.H., 2010. Disposition of charged nanoparticles after
818 their topical application to the skin. Skin Pharmacol Physiol. 23, 117-123.
819
820 Yin, T., Wang, P., Li, J., Wang, Y., Zheng, B., Zheng, R., Cheng, D., Shuai, X., 2014. Tumor-
821 penetrating codelivery of siRNA and paclitaxel with ultrasound-responsive nanobubbles hetero-
822 assembled from polymeric micelles and liposomes. Biomaterials 35(22), 5932-5943.
823
824 Yu, H., Chen, S., Cao, P., 2012. Synergistic bactericidal effects and mechanisms of low intensity
825 ultrasound and antibiotics against bacteria: a review. Ultrasonics sonochemistry 19(3), 377-382.
826
827 Zilberman, M., Elsner, J.J., 2008. Antibiotic-eluting medical devices for various applications. J Control
828 Release 130(3), 202-215. doi: 10.1016/j.jconrel.2008.05.020. Epub 2008 Aug 6. Review. PubMed
829 PMID: 18687500.

Figure legends

Figure 1. **Schematic structure of VmLNB formulations.** Vm nanocarriers described in the present work display a core-shell structure. PFP was employed as core fluorocarbon, whereas dextran sulfate was chosen as polysaccharidic shell molecule. Vm was inserted into the outer shell throughout dextran sulfate chains. In selected experiments, VmLNBs were further functionalized by including fluorescent 6-coumarin in the inner core.

Figure 2. NB and VmLNB morphology. NBs and VmLNBs were checked for morphology by TEM. Results are shown as representative images from three different preparations. Panel A. NB image by TEM. Panel B. VmLNB image by TEM. (see also Figure S1 in Supplementary Materials for additional images of multiple nanobubbles within the same field).

Figure 3. Stability of Vm and VmLNB formulations. The stability of Vm solution and VmLNB suspension was monitored up to 14 days either at room temperature (Panel A) or at 37°C (Panel B) through analysis by HPLC. Results are shown as means ± SD from three different preparations for each formulation. Data were also analyzed for significance by ANOVA. Versus Vm solution: * $p<0.001$.

Figure 4. Biocompatibility of Vm and VmLNBs with human keratinocytes *in vitro*. HaCaT cells (10^6 cells/2 mL DMEM medium implemented with 10% FCS) were left untreated (ctr) or treated with 200 μL of Vm solution or VmLNB suspension for 24 h in normoxia (20% O_2). Thereafter, Vm and VmLNB cytotoxicity were measured through LDH assay (Panel A), whereas cell viability was measured through MTT assay (Panel B). Results are shown as means ± SEM from three independent

853 experiments. Data were also evaluated for significance by ANOVA. No significant differences were
854 found among all conditions.

855 **Figure 5. *In vitro* Vm release from Vm and VmLNB formulations.** Vm release from Vm solution
856 and VmLNB suspension was monitored up to 6 h. Results are shown as means ± SD from three
857 different preparations for each formulation. Data were also analyzed for significance by ANOVA.
858 Versus Vm solution: * $p<0.001$.

859

860 **Figure 6. Antibacterial activity of Vm and VmLNBs against MRSA.** MRSA were left for 2, 3, 4, 6
861 and 24 hours at 37°C alone (ctr) or incubated with 10% v/v NBs or different concentrations of Vm,
862 either free or loaded on VmLNBs (Panel A: 1 mg/mL; Panel B: 0.1 mg/mL; Panel C: 0.01 mg/mL;
863 Panel D: 0.004 mg/mL). Results are shown as means ± SEM from three independent experiments. Data
864 on Vm- and VmLNB-treated samples were normalized upon Vm/VmLNB release ratios reported in
865 Table 2 (see also in Supplementary Materials: Table S3 for further information on percentages of drug
866 release from VmLNBs at different times/concentrations; and Figure S2 for raw data on VmLNB
867 antibacterial effects). All data were also evaluated for significance by ANOVA. Versus ctr: * $p < 0.02$;
868 versus Vm: ° $p < 0.05$.

869

870 **Figure 7. Drug loading on dextran sulfate-shelled NBs prevents Vm internalization by MRSA.**
871 MRSA were left alone or incubated with 10% v/v 6-coumarin-labeled VLNBs, 6-coumarin-labeled
872 NBs, and FITC-labeled Vm for 2h at 37°C. After staining bacteria with PI, confocal fluorescent images
873 were taken using FITC and TRITC filters. Data are shown as representative images from three
874 independent experiments. Magnification: 100X. Red: PI. Green: 6-coumarin or FITC.

875

Figure 8. US-triggered sonophoresis of VmLNBs through skin membranes. US (t = 10 min; f = 2.5 MHz; P = 5 W) abilities to induce sonophoresis and Vm permeation from VmLNBs were evaluated up to 6 h by using a vertical diffusion Franz cell consisting in two chambers (donor and recipient, respectively) separated by a pig skin layer (see scheme in Panel A). Results are shown in Panel B as means ± SD from three independent experiments. Data were also evaluated for significance by ANOVA. Versus without US: $p < 0.001$.

Tables and legends

Formulation	Average diameter ± SD (nm)	Polydispersity index	Zeta Potential ± SD (mV)	Viscosity (cP)
NBs	313.4 ± 26.4	0.24 ± 0.02	- 34.5 ± 0.38	1.22
VmLNBs	304.6 ± 14.6	0.22 ± 0.03	- 28.6 ± 1.34	1.25
Fluorescent NBs	312.8 ± 22.7	0.25 ± 0.02	- 34.1 ± 1.22	1.24
Fluorescent VmLNBs	308.9 ± 22.4	0.23 ± 0.01	- 29.5 ± 1.88	1.23

Table 1. Physical-chemical characterization of NBs and VmLNBs. Liquid formulations were characterized for average diameters, polydispersity index, and zeta potential by light scattering. The viscosity (cP) of NB and VmLNB suspensions was determined at 25 °C by using a Ubbelohde capillary viscosimeter. Results are shown as means ± SD from three preparations. See also Figures 1-2 for further detail on NB and VmLNB structure and morphology.

time (hours)	% drug release from Vm solution	% drug release from VmLNBs	Vm/VmLNB drug release ratio
2	36.57	5.99	6.11
3	45.97	7.97	5.78
4	57.16	10.27	5.57
6	73.44	14.59	5.03
24	92.34	35.84	2.58

Table 2. *In vitro* drug release from Vm solution and VmLNB suspension. After incubation for increasing times (first column), the percentages of *in vitro* drug release from Vm solution (second column) and VmLNB suspension (third column) were measured. Then, Vm/VmLNB drug release ratios (fourth column) were calculated for each time considered. All incubation times (2, 3, 4, 6, and 24 h) were purposely chosen to further normalize the results from the experiments with MRSA (see Figure 6). Results are shown as mean values from three different preparations for each formulation.

Vancomycin-loaded nanobubbles: a new platform for controlled antibiotic delivery against methicillin-resistant *Staphylococcus aureus* infections.

Monica Argenziano[1], Giuliana Banche[2,*], Anna Luganini[3], Nicole Finesso[4], Valeria Allizond[2], Giulia Rossana Gulino[4], Amina Khadjavi[4,5], Rita Spagnolo[1], Vivian Tullio[2], Giuliana Giribaldi[4], Caterina Guiot[5], Anna Maria Cuffini[2], Mauro Prato[2,5,§], Roberta Cavalli[1, §,*]

[1] *Dipartimento di Scienza e Tecnologia del Farmaco, Università degli Studi di Torino, Torino, Italy*

[2] *Dipartimento di Scienze della Sanità Pubblica e Pediatriche, Università degli Studi di Torino, Torino, Italy*

[3] *Dipartimento di Scienze della Vita e Biologia dei Sistemi, Università degli Studi di Torino, Torino, Italy*

[4] *Dipartimento di Oncologia, Università degli Studi di Torino, Torino, Italy*

[5] *Dipartimento di Neuroscienze, Università degli Studi di Torino, Torino, Italy*

§ Equal contribution to the work

* Corresponding authors:

Prof. Roberta Cavalli, Dipartimento di Scienza e Tecnologia del Farmaco, Università degli Studi di Torino, via P. Giuria 9, 10125 Torino, Italy. Phone no.: +39-011-6707686. Fax no.: +39-011-6707687. E-mail address: roberta.cavalli@unito.it

Dr. Giuliana Banche, Dipartimento di Scienze della Sanità Pubblica e Pediatriche, Università degli Studi di Torino, Via Santena 9, 10126 Torino, Italy. Phone no.: +39-011-6705627. Fax no.: +39-011-2365627. E-mail address: giuliana.banche@unito.it

Abstract

Vancomycin (Vm) currently represents the gold standard against methicillin-resistant *Staphylococcus aureus* (MRSA) infections. However, it is associated with low oral bioavailability, formulation stability issues, and severe side effects upon systemic administration. These drawbacks could be overcome by Vm topical administration if properly encapsulated in a nanocarrier. Intriguingly, nanobubbles (NBs) are responsive to physical external stimuli such as ultrasound (US), promoting drug delivery. In this work, perfluoropentane (PFP)-cored NBs were loaded with Vm by coupling to the outer dextran sulfate shell. Vm-loaded NBs (VmLNBs) displayed ~300 nm sizes, anionic surfaces and good drug encapsulation efficiency. *In vitro*, VmLNBs showed prolonged drug release kinetics, not accompanied by cytotoxicity on human keratinocytes. Interestingly, VmLNBs were generally more effective than Vm alone in MRSA killing, with VmLNB antibacterial activity being more sustained over time as a result of prolonged drug release profile. Besides, VmLNBs were not internalized by *staphylococci*, opposite to Vm solution. Further US association promoted drug delivery from VmLNBs through an *in vitro* model of porcine skin. Taken together, these results support the hypothesis that proper Vm encapsulation in US-responsive NBs might be a promising strategy for the topical treatment of MRSA wound infections.

Key words

Nanobubbles; vancomycin; methicillin-resistant *Staphylococcus aureus*; ultrasound; prolonged release.

1. Introduction

Chronic wounds fail to proceed through timely regulated and interrelated processes to restore anatomical and functional integrity of the injured tissues (Lazarus et al., 1994) such as diabetic feet, bedsores, and venous ulcers (Markova et al., 2012). To date, these types of wounds are considered like a silent epidemic, affecting a large fraction of the world population and posing a major gathering threat to the public health and economy of all developed countries (Daeschlein, 2013). Hospitalized patients are at particular risk, especially those suffering from diabetes, human immunodeficiency virus or other immune disorders, as well as those undergoing chemotherapy (Payne et al., 2008).

Beyond delayed healing processes due to different factors (hypoxia, persistent inflammation, and altered balances between tissue remodelling proteinases and their inhibitors), chronic wounds are often worsened by microbial infections (Gurusamy et al., 2013). Among the bacteria responsible for skin infection, *Staphylococcus aureus* represents the most common pathogen to be identified in chronic wounds, with methicillin-resistant *S. aureus* (MRSA) accounting for upward of 20% to 50% of cases (Price, 2010). MRSA colonies often develop at the interface between synthetic prostheses and biological tissues, particularly during surgery and post-surgery course. In addition, MRSA colonization or infection of wounds can result in MRSA bacteremia, which is associated with a 30-day mortality of about 28% to 38% patients (Gurusamy et al., 2013).

The main goal of chronic wound treatment is to decrease the injuring-associated microbial load, thus allowing wound healing processes to take place. However, conventional systemic delivery of antibiotics not only entails poor penetration into ischemic and necrotic tissues, but can also cause systemic toxicity with associated renal and liver complications, resulting in forced hospitalization for further monitoring and advanced treatment. On the contrary, topically applied antimicrobials have

proven effective in decreasing bacterial levels in granulating wounds (Diehr et al., 2008~~7~~). Therefore, alternative local delivery of antimicrobials - either by topical administration or through novel delivery devices - may enable to keep high local antibiotic concentrations for prolonged release times without reaching systemic toxicity (Zilberman et al., 2008).

A promising approach to develop a topical therapy for microbial infection in skin and soft tissues would employ biocompatible nanomaterials and drug nanocarriers. Indeed, nanotechnology represents an emerging field to be exploited for antibiotic drug delivery. Thanks to their physical and chemical properties (small size, high surface-to-volume ratio and suitable surface modification) nano-sized materials may be used as drug carriers to trespass several physiological barriers and to reach biological targets. The coupling of nanocarriers with anti-infectious agents makes it likely to increase drug concentrations and drug penetration at the site of infection. As a result, it might not only improve the therapeutic index but also reduce some issues associated with nonspecific cytotoxicity and antibiotic resistance (Sharma et al., 2012).

Vancomycin hydrochloride, being effective against many Gram-positive bacteria that are unresponsive to common antibiotics, represents the gold standard against MRSA infections (Kullar~~rrant~~ et al., 2016). However, Vm is poorly absorbed from the gastrointestinal tract with a low oral bioavailabiliy. Low intravenous infusion is often suggested as a feasible alternative for drug administration, but Vm instability in aqueous solutions at 37°C could imply a tremendous reduction of drug effectiveness (Mawhinney et al., 1992; Raverdy et al., 2013). Following parenteral administration, Vm displays a slow mode of action, a complex concentration-time profile, and a disappointingly low penetration in tissues (Vandecasteele et al., 2012). Furthermore, systemic Vm administration can be associated with several adverse effects (Vidal et al., 1992). On the other hand, Vm topical application – that would be much safer than systemic administration - is currently limited by several factors such as skin barrier properties and poor drug permeability (Giandalia et al., 2001). Being the main goal of chronic wound

treatment to decrease the microbial load, allowing the healing processes to take place, new delivery protocol should be devised, since conventional systemic delivery of antibiotics requires a drug concentration which is locally ineffective because of the poor penetration into ischemic and necrotic tissues, but can cause systemic toxicity and topically applied antimicrobials have proven effective in decreasing bacterial levels in granulating wounds (Diehr et al., 2007), without inducing systemic toxicity (Zilberman et al., 2008) but suffer from poor diffusion across membranes.

Intriguingly, the use of a nanocarrier may help to avoid the abovementioned drawbacks. Notably, nanocarriers such as liposomes, microemulsions, and lipid nanoparticles have the potential to deliver drugs to the skin more efficiently than conventional topical carriers such as creams and ointments, that are not usually recommended for applications on injured skin (Giandalia et al., 2001; Prabhu et al., 2012). However, the response to drug topical applications has been too weak so far, mainly due to the inability to cross the external skin barrier (*stratum corneum*) and reach the dermal regions where the bacteria are nested. Interestingly, physical media such as ultrasound (US) are reportedly able to trigger drug release at the site of infection by temporarily increasing skin permeability through sonophoresis. As such, US is useful to promote drug targeting and transdermal delivery in a non-invasive manner (Azagury et al., 2014; Park et al, 2012).

Microbubbles (MBs) (Guiot et al., 2006), nanobubbles (NBs) (Cavalli et al., 2009a; Cavalli et al., 2009b; Cavalli et al., 2016) and nanodroplets (NDs) (Magnetto et al., 2014; Prato et al., 2015) are suitable carriers to be combined with such a physical trigger. They are spherical core-shell structures filled with gases such as perfluorocarbons. Particularly, oxygen-cored nanostructures can be employed both for sonography (as contrast agents) (Fokong et al., 2012; Marxer et al., 2011) and for therapy (as hypoxia- and infection-counteracting devices) (Gulino et al., 2015; Banche et al., 2015; Khadjavi et al., 2015; Basilico et al., 2015; Prato et al., 2016). In particular NBs, consisting in an outer shell of a biocompatible/biodegradable polysaccharide (chitosan, dextran, or dextran sulfate) and an inner core

filled with an oxygen-storing fluorocarbon (perfluoropentane, PFP), have been purposely developed as a new non-invasive, low-cost and multipurpose nanotechnological platform (Cavalli et al., 2009a; Cavalli et al., 2009b; Cavalli et al., 2016). PFP is a perfluorocarbon with a boiling point of 29°C, hence liquid at room temperature. The use of PFP allows liquid droplet generation at room temperature. Then, PFP in nanodroplets can be activated by an external stimulus, like US, by means of a mechanism called acoustic droplet vaporization, causing the droplet to become a bubble. Depending on the properties of the nanostructure, NBs can be subsequently coupled with different molecules, such as drugs or genetic materials, thus acting as nanocarriers (Cavalli et al., 2012; Cavalli et al., 2013; Delalande et al., 2012; Yin et al., 2014). Due to their structure and their gaseous core, NBs are very responsive to US and can take advantage from a number of effects related to microcavitation and microstreaming, occurring at the liquid-membrane interface and responsible for transitory and reversible openings of the pores, thus crossing the membrane itself and delivering their content beyond the tissue (sonophoresis) or the cell (sonoporation) membrane (Karshafian et al., 2009).

Based on these preconditions, the present work aimed at producing dextran sulfate-shelled and PFP-cored NBs for Vm local delivery to potentially treat skin infectious diseases. The formulation is referred to as "nanobubbles" for sake of simplicity but it must be said that, prior to the application of US, it would be more accurate to use the term "nanodroplets" when the core is constituted of PFP. Therefore, Vm-loaded NBs (VmLNBs) were prepared and characterized for physico-chemical parameters and drug release kinetics; tested for biocompatibility with human skin cells and for their antibacterial properties or interactions with MRSA; and challenged for responsiveness to US, in order to assess their effectiveness as Vm nanocarriers for local delivery.

2. Material and methods

2.1. Materials

All materials were from Sigma-Aldrich, St Louis, MO, unless those indicated as follows. Sterile plastics were from Costar, Cambridge, UK; ethanol (96%) was from Carlo Erba (Milan, Italy); soybean lecithin (Epikuron 200®) was from Cargill (Hamburg, Germany); 1-800 Millipore system to obtain ultrapure water and Amicon® Ultra-0.5 centrifugal filter device were from Millipore (Molsheim, France); Ultra-Turrax SG215 homogenizer was from IKA (Staufen, Germany); RPMI 1640 medium was from Invitrogen (Carlsbad, CA); Nanobrook 90Plus Particle Size Analyzer was from Brookhaven (New York City, NY); Philips CM10 electron microscope was from Philips (Eindhoven, the Netherlands); Ubbelhode capillary viscosimeter was from SCHOTT Instruments GmbH (Mainz, Germany); Perkin Elmer PUMP 250B was from Perkin Elmer (Waltham, MA); Flexar UV/Vis LC spectrophotometer detector was from Perkin Elmer (Waltham, MA); Agilent TC C_{18} columns were from Agilent (Santa Clara, CA); Orion Model 420A pH Meter was from Thermo Scientific (Waltham, MA); Semi-Micro Osmometer K-7400 was from Knauer (Berlin, Germany); Beckman Coulter Allegra 64R Centrifuge was from Beckman Coulter (Brea, CA); Spectra/Por cellulose membranes were from Spectrum Laboratories (Rancho Dominguez, CA); HaCaT cells were from Cell Line Service GmbH (Eppelheim, Germany); cell culture RPMI 1640 and Dulbecco's modified Eagle's medium (DMEM) were from Invitrogen (Carlsbad, CA); streptomycin was from Cambrex Bio Science (Vervies, Belgium); humidified CO_2/air-incubator was from Thermo Fisher Scientific Inc. (Waltham, MA); tryptic soy broth (TSB) and tryptic soy agar (TSA) were from Merk KgaA (Darmstadt, Germany); Olympus Fluoview 200 laser scanning confocal system mounted on an inverted IX70 Olympus microscope was from Olympus America Inc. (Melville, NY, USA) ; SPSS 16.0 software was from SPSS Inc. (Chicago, IL).

2.2. Development and manufacturing of formulations

2.2.1. Determination of Vm and dextran sulfate interaction ratio

Increasing concentrations (0.25, 0.5, 1.0, 2.0 mg/mL) of dextran sulfate aqueous solutions (1 mL) were added to 1 mL of Vm aqueous solution (1 mg/mL) under magnetic stirring at room temperature overnight. After equilibration, the systems were separated by centrifugation (20000 rpm, 15 minutes) using a centrifugal filter device (Amicon® Ultra), in order to determine the amount of unbound Vm in the filtrate phase. The drug concentration in the filtrate was determined using the HPLC method described below.

2.2.2. Preparation of NB, Vm, and VmLNB formulations

NBs were formulated using PFP for the inner core and dextran sulfate for the shell. A purposely tuned multi-step protocol was designed. Briefly, a pre-emulsion was obtained adding 300 µ~~m~~L of an ethanol solution containing Epikuron® 200 and palmitic acid (1% w/v) to 500 µL of PFP under magnetic stirring. After the addition of 4.8 mL of ultrapure water, the system was homogenized using a Ultra-Turrax SG215 homogenizer. To obtain the polymeric NBs, 350 µL of 1% w/v dextran sulfate (molecular weight = 100 kDa) aqueous solution was added drop-wise under magnetic stirring. Blank NBs obtained according to this procedure were employed as control formulations in the subsequent experiments. On the other hand, to obtain VmLNBs, an extra step based on drop-wise addition of a Vm aqueous solution (pH 3.5) to the so-formed NBs was performed under mild stirring. Different concentrations of Vm solutions were added to prepare a series of VmLNB formulations with increasing drug content (0.004, 0.01, 0.1, and 1 mg/mL). VmLNBs were then purified by dialysis to eliminate

unbound molecules. For selected experiments, fluorescent NBs and VmLNBs were obtained by the addition of 6-coumarin (1 mg/mL) to the PFP core. Alternatively, fluorescent Vm was synthesized through reaction between fluorescein isothiocyanate (FITC) and Vm. For this purpose, an amount of FITC solution in methanol (0.2 % w/v) was added to Vm aqueous solution and incubated under stirring overnight in the dark. **Figure 1** shows a representative scheme resuming the general structure of fluorescent VmLNBs. For cell experiments, NBs were prepared in phosphate buffer saline pH 7.4 (PBS). For *in vitro* permeation studies, NBs were prepared in saline solution (NaCl 0.9% w/v).

Formatted: Font: Italic

2.2.3. NB sterilization

Firstly, the glassware and the components were sterilized at 121 °C and 2 bar. Subsequently, all NB formulations were sterilized through UV-C exposure for 20 min. Thereafter, UV-C-treated materials were incubated with cell culture RPMI 1640 medium in a humidified CO_2/air-incubator at 37°C up to 72 h, not displaying any signs of microbial contamination when checked by optical microscopy.

2.3. Characterization of formulations

2.3.1. Characterization of NB and VmLNB formulations

The average diameter, polydispersity index and zeta potential were determined by photocorrelation spectroscopy using a particle size analyzer at a scattering angle of 90° and a temperature of 25 °C. NB suspensions were diluted in deionized filtered water before measurement. For zeta potential determination, samples of diluted NB formulations were placed in the electrophoretic cell, where an electric field of approximately 15 V/cm was applied. The morphology of formulations was evaluated by Transmission Electron Microscopy (TEM), using a Philips CM10 (Eindhoven, NL) instrument. NB and VmLNB aqueous suspensions were sprayed on Formwar-coated copper grid and air-dried before

observation. The viscosity of the samples was determined at 25 °C using a Ubbelhode capillary viscosimeter.

2.3.2. HPLC quantitative Vm determination

Vm quantitative determination was carried out by using an HPLC system based on a Perkin Elmer pump equipped with a spectrophotometer detector. Analyses were performed using an Agilent TC C_{18} column (250 mm × 4.6 mm, 5 µm). The mobile phase was a mixture of KH_2PO_4 50 mM (pH 4) and acetonitrile (92:8 v/v), degassed and pumped through the column with a flow rate of 1 mL/min. Ultraviolet detection was set at 286 nm. The external standard method was used to calculate the drug concentration. For this purpose, 1 mg of Vm was weighted, placed in a volumetric flask, and dissolved in water to obtain a stock standard solution. This solution was then diluted using the mobile phase, providing a series of calibration solutions, subsequently injected into the HPLC system. Linear calibration curve was obtained over the concentration range of 0.5−25 µg/mL, with a regression coefficient of 0.999.

2.3.3. In vitro evaluation of Vm stability

Vm chemical stability - either solved in aqueous solution or loaded in VmLNBs - was evaluated at room temperature and at 37 °C over time. A quantitative determination of Vm concentration over time was carried out using the HPLC method described above.

2.3.4. NB stability over time and after US administration

The physical stability of NBs was evaluated by morphological analysis and by size and zeta potential determination of formulation over time. Their average diameters, zeta potential values and morphology were assessed up to six months. Stability was also investigated following NB exposure to US (f = 2.5±

0.1 MHz; t = 10 min; P = 5 W). NB morphology was observed by TEM to confirm the integrity of NB structure.

2.3.5. Encapsulation efficiency and loading capacity of Vm in NBs

The encapsulation efficiency of VmLNBs was determined using a centrifugal filter system. 150 µ~~micro~~L of VmLNB suspension were put in an Amicon® Ultra-0.5 centrifugal filter device and centrifuged at 15000 rpm for 30 minutes using Beckman Coulter Allegra 64R Centrifuge. The solution filtered in the bottom of the tube was quantified and after suitable dilution was analyzed by HPLC, in order to obtain the concentration of free Vm in VmLNBs suspensions. The encapsulation efficiency was calculated by subtracting the amount of free drug from the initial amount of added Vm, according to the following equation:

$$Encapsulation\ efficiency = \frac{(total\ Vm - free\ Vm)}{total\ Vm} \times 100$$

The loading capacity was determined on freeze-dried NB samples. Briefly, a weighted amount of freeze-dried VmLNBs was suspended~~diluted~~ in 10~~5~~ mL of water. After sonication and centrifugation, the supernatant was diluted with mobile phase and analyzed by HPLC. The loading capacity of Vm in VmLNBs was calculated as follows:

$$Loading\ capacity = \frac{(total\ Vm - free\ Vm)}{NB\ weight} \times 100$$

2.4. *In vitro* release studies

In vitro drug release experiments were conducted in a multi-compartment rotating cell, comprising a donor chamber separated by a cellulose membrane (cut-off = 12000 Da) from a receiving compartment. One ml of VmLNB suspension at different concentrations (1, 0.1, 0.01 and 0.004 mg/mL) was placed

in the donor chamber. The *in vitro* release kinetics of Vm from VmLNB was compared to a Vm aqueous solution (1 mg/mL) as a control. The receiving phase, containing phosphate buffer 0.05 M (pH 7.4) was withdrawn at regular intervals and replaced with the same amount of fresh buffer. Quantitative determination of Vm in the withdrawn samples was carried out by the HPLC method, as described in the previous paragraph. Data were expressed as % of Vm released over time.

2.5. *In vitro* permeation study

In vitro studies were performed using a vertical diffusion Franz cell to evaluate Vm permeation throughout the skin. The Franz cell consists of a donor compartment, with Vm (1 mg/mL, either free or carried by VmLNBs, $1x10^{12}$ NBs/ml) and a receiving compartment containing 0.9% w/w NaCl saline solution. To simulate the *stratum corneum* properties a membrane pig ear skin was used. Skin slices were isolated with a dermatome from the outer side of pig ears, obtained from a local slaughterhouse, and then were frozen at −18 °C. Before starting the experiments, the skin was equilibrated in NaCl 0.9 % w/w saline solution, in the presence of 0.01% sodium azide to preserve the skin, at 25 °C for 30 min. Then, after washing with saline solution, the skin layer was inserted between the two compartments of the Franz cell, with the stratum corneum side facing towards the donor chamber. The study was carried out for 24 hours and the receiving phase was withdrawn at regular times and replaced with the same amount of fresh receiving medium. The collected samples were then analyzed by HPLC to determine the amount of Vm permeated over time. US abilities to promote Vm permeation were also investigated. For this purpose, a high frequency US transducer (f = 2.5 MHz; P = 5 W; t = 10 min) was combined to a purposely modified vertical diffusion cell. Drug permeation through pig skin after US application was monitored by HPLC analysis of the cumulative amount of antibiotic reaching the receiving phase over time.

Formatted: Superscript

Formatted: Font: Italic

2.6. Human biocompatibility studies

2.6.1. Human keratinocyte cell cultures

HaCaT, a long-term cell line of human keratinocytes immortalized from a 62-year old Caucasian male donor (Boukamp et al., 1988), was used for the assessment of Vm and VmLNB biocompatibility. Cells were grown as adherent monolayers in DMEM medium supplemented with 10% fetal bovine serum, 100 U/mL penicillin, 100 µg/mL streptomycin and 2 mM L-glutamine in a humidified CO_2/air-incubator at 37°C. Before starting the experiments, cells were washed with PBS, detached with trypsin/ethylenediaminetetraacetic acid (0.05/0.02 % v/v), washed with fresh medium and plated at a standard density (10^6 cells/well in 6-well plates) in 2 mL of fresh medium.

2.6.2. Vm and VmLNB cytotoxicity

The potential cytotoxic effects of VmLNBs were measured as the release of lactate dehydrogenase (LDH) from HaCaT cells into the extracellular medium. Briefly, cells were incubated in DMEM medium for 24 h with/without 1 mg/mL Vm, either free or carried by VmLNBs, in a humidified CO_2/air-incubator at 37°C. Then, 1 mL of cell supernatants was collected and centrifuged at 12000 rpm~~13000*g*~~ for 2 min. Cells were washed with fresh medium, detached with trypsin/ethylenediaminetetraacetic acid (0.05/0.02 % v/v), washed with PBS, resuspended in 1 mL of TRAP (82.3 mM triethanolamine, pH 7.6), and sonicated on ice with a 10 s burst. 5 µ~~micro~~L of cell lysates and 50 ~~micro~~µL of cell supernatants were diluted with TRAP and supplemented with 0.5 mM sodium pyruvate and 0.25 mM NADH (300 µ~~micro~~L as a final volume) to start the reaction. The reaction was followed measuring the absorbance at 340 nm (37 °C) with Synergy HT microplate reader. Both intracellular and extracellular enzyme activities were expressed as µmol of oxidized

NADH/min/well. Finally, cytotoxicity was calculated as the net ratio between extracellular and total (intracellular + extracellular) LDH activities.

2.6.3. Human keratinocyte cell viability

Cell viability was evaluated using 3-(4,5-dimethylthiazol-2-yl)-2,5-diphenyltetrazolium bromide (MTT) assay. HaCaT cells were incubated for 24 h with/without 1 mg/mL Vm, either free or carried by VmLNBs, in a humidified CO_2/air-incubator at 37°C. Thereafter, 20 ~~micro~~µL of 5 mg/mL MTT in PBS were added to cells for 3 additional hours at 37 °C. The plates were then centrifuged, the supernatants discarded and the dark blue formazan crystals dissolved using 100 µL of lysis buffer containing 20 % (w/v) sodium dodecyl sulfate, 40 % N,N-dimethylformamide (pH 4.7 in 80 % acetic acid). The plates were then read on Synergy HT microplate reader at a test wavelength of 550 nm and at a reference wavelength of 650 nm.

2.7. Microbiological assays

2.7.1. Determination of vancomycin antimicrobial activity against MRSA

Vm solutions were freshly prepared for each experiment. Determination of the minimum inhibitory concentration (MIC) of vancomycin was carried by the microdilution broth method according to the latest Clinical and Laboratory Standards Institute (CLSI) guidelines (CLSI 2012). Interpretation of the results was performed as outlined in the above mentioned CLSI guidelines (CLSI 2012).

2.7.2. In vitro antibacterial efficiency of VmLNBs against MRSA.

MRSA, isolated from human ulcerated wounds (Infermi Hospital, Biella, Italy), was cultured over night at 37°C in TSB. After incubation, bacteria were re-suspended in 100 mL of TSB, harvested by 10

min centrifugation at 4,000 rpm, diluted in TSB to 10^4 colony-forming-unit (CFU)/mL, as confirmed by colony counts on TSA, and then incubated in TSB with VmLNBs, loaded with Vm at different concentrations (1, 0.1, 0.01, and 0.004 mg/mL), in sterile sampling tubes for 2, 3, 4, 6, and 24 hours at 37°C. Controls represented by either bacteria incubated in TSB, bacteria incubated with blank NBs or bacteria incubated in the presence of free Vm at different concentrations (1, 0.1, 0.01 and 0.004 mg/mL), were also performed. At each incubation time, serial 10-fold dilutions in saline solution (0.9% NaCl) were prepared from each sample, and 100 µ~~micro~~L of each dilution were spread on TSA, so that the number of CFU/mL could be determined.

2.7.3. Imaging with confocal laser scanning microscopy

MRSA bacteria ~~*S. aureus* strain~~ were~~was~~ grown in TSB at 37°C in agitation until reaching the concentration of 1x10^^{9} CFU/mL. Then, 1 mL aliquot of bacteria was pelleted (3000g x 10 min at 4°C), resuspended in PBS 1x and incubated with 6-coumarin-labeled VmLNBs, 6-coumarin-labeled NBs, or FITC-labeled Vm at a dilution of 1:11, as for previous experiments performed on eukaryotic cells. Each sample was placed on orbital shaker (160 rpm) in the dark at 37°C for 2h and 4h. After incubation, one drop from each suspension was streaked on poly-L-lysine-coated microscope slides and allowed to dry. Then, bacteria were stained with iodide propidium (PI) in PBS 1X and again allowed to dry. Fluorescence images were taken with an Olympus IX70 inverted laser scanning confocal microscope, and captured using FluoView 200 software.

2.8. Statistical analysis

At least three independent experiments, each one in duplicate or triplicate, were performed for every investigational study. Numerical data are shown as means ± SEM for inferential results or as means ± SD for descriptive results (see Cumming et al., 2007 for an exhaustive review). Imaging data are shown

as representative pictures. All data were analyzed by a one-way Analysis of Variance (ANOVA) followed by Tukey's post-hoc test (software: SPSS 16.0 for Windows, SPSS Inc., Chicago, IL). $P<0.05$ were considered significant.

3. Results

3.1. Characterization of VmLNB and control (blank NB and Vm) formulations

Before NB production, the interaction between dextran sulfate and Vm was firstly investigated to optimize Vm/dextran sulfate ratio. Results indicated that Vm was complexed at 99% by dextran sulfate solution until the concentration of 0.5 mg/mL~~l~~ (data not shown). The Vm/dextran sulfate ratio was calculated corresponding to 2:1 (w/w). Based on this preliminary information, NBs were prepared according to the protocol described in the Materials and Methods section. After manufacturing, VmLNB and blank NB formulations (with or without 6-coumarin in the inner core) were characterized physico-chemically. Results are shown in **Figure 2** and **Table~~s~~ 1~~ 2~~**. Both VmLNBs and NBs displayed spherical shapes with a core-shell structure by TEM analyses. All sizes were in the nanometer range, with all formulations displaying around 300 nm as a value for average diameters. All polidispersity indexes were included between 0.22 and 0.25. Zeta potentials ranged from -34 mV (NBs) to -29 mV (VmLNBs). The loading of Vm in the NB structure did not significantly affect the viscosity of the formulations. ~~NB viscosity (1.12 cP) was slightly increased upon binding with Vm (1.25 cP for VmLNBs).~~ NBs were able to load Vm with an encapsulation efficiency of 86% and loading capacity of 29%.

3.2. Stability of VmLNB and control (blank NB and Vm) formulations

NB and VmLNB formulations proved to be physically stable over time, as confirmed by long-term checking of the parameters assessed in the previous paragraph. Indeed, the obtained values did not remarkably change up to six months after the manufacturing of the formulations stored at 4 °C (data not shown). Furthermore, the chemical stability of the drug was comparatively checked between free Vm solution and VmLNB aqueous suspension either over time (up to 14 days) or at different

temperatures (25°C and 37°C). As shown in **Figure 3**, the drug ~~Vm always~~ resulted much more stable from a chemical point of view when properly incorporated in the nanocarrier~~s~~ (VmLNBs) than as such in solution.~~alone.~~

3.3. Human biocompatibility

The potential toxicity of Vm solution and VmLNB suspension on human skin cells was assessed by testing *in vitro* cultured HaCaT keratinocytes. Cells were incubated for 24 h alone, with 10% v/v Vm solution, or with VmLNB nanosuspensions in normoxic conditions (20% O_2). Thereafter, cytotoxicity was analyzed by LDH assay, and cell viability by MTT assay. As shown in **Figure 4**, neither Vm nor VmLNBs did show significant toxic effects and HaCaT cell viability was not significantly affected by either formulation.

3.4. *In vitro* drug release from VmLNBs

In vitro drug release from VmLNB nanosuspension and free Vm solution were comparatively evaluated over time. As shown in **Figure 5** (time course studies up to 6 h) and **Table 2~~3~~** (end-point data up to 24 h), 1 mg/mL Vm release from VmLNBs was slow and prolonged over time, compared to free drug solution diffusion. No initial burst effect was observed indicating Vm incorporation in NB shell. Further information on additional incubation times and drug concentrations for VmLNBs is available in Supplementary Materials (**Table S3~~1~~**). Vm/VmLNB drug release ratios at different times (2, 3, 4, 6, and 24 h) were also calculated (see **Table 2~~3~~**), in order to allow normalization of the results from treatment with VmLNBs in the microbiological experiments described in the following paragraph.

3.5. *In vitro* antimicrobial activity of VmLNBs

According to preliminary microbiological analyses performed on the MRSA strain employed in the present experiments, 0.004 mg/mL resulted as the MIC value for Vm. Therefore, decreasing Vm concentrations from 1 mg/mL (used for the studies described in the previous paragraphs) to 0.004 mg/mL (MIC value) were employed in a series of experiments aimed at comparatively evaluating Vm (either free or carried by VmLNBs) antibacterial effectiveness against MRSA. Bacteria were incubated at different times (2, 3, 4, 6, and 24 h) either alone (ctr) or with free Vm, VmLNBs, or blank NBs. The initial drug concentrations (1; 0.1; 0.01; and 0.004 mg/mL) loaded on VmLNBs were the same as those solved in free Vm solution. However, as emerged in the previous paragraph, drug release from VmLNBs is significantly slower than free Vm solution diffusion. For this reason, before proceeding with the analysis of the results, all values on bacterial growth referring to Vm- and VmLNB-treated samples were normalized upon time-dependent Vm/VmLNB drug release ratios shown in **Table 2~~3~~**. Normalized results are shown in **Figure 6**, whereas raw data are available in Supplementary Materials (**Figure S2~~4~~**). 1 mg/mL Vm effectively inhibited bacterial growth at all times, independently from being free or carried by the nanocarrier. Lower drug concentrations of free Vm solution were effective against MRSA only after longer times of incubation (at least 3 h for 0.1 mg/mL and 0.01 mg/mL Vm; and at least 4 h for 0.004 mg/mL Vm). Interestingly, Vm antibacterial efficacy was significantly improved when the drug was carried by VmLNBs. Indeed, VmLNB-dependent inhibition of bacterial growth was significantly enhanced compared to free Vm solution, at all drug concentrations. Additionally, compared to free Vm solution, VmLNB antibacterial effects appeared earlier, as they were already evident after 2 h of incubation (the first time-point of the observational period) at all Vm concentrations. Blank NBs did not show any antibacterial activity.

Further analysis by confocal microscopy (**Figure 7**) displayed that MRSA avidly internalized free fluorescent Vm already after 2 h of incubation, but not fluorescent VmLNBs. Fluorescent Vm-free NBs did adhere to the bacterial cell wall without being internalized.

3.6. US-triggered drug permeation

The ability of US to promote Vm permeation through the skin was assayed by employing a purposely modified Franz cell constituted by a donor and a recipient chamber separated by a pig skin layer (see **Figure 8A** for a schematic representation of the apparatus). As shown in **Figure 8B**, the administration of US (t = 10 min; f = 2.5 MHz; P = 5 W) strongly induced VmLNBs to deliver the antibiotic drug from the donor chamber throughout the pig skin membrane into the recipient chamber up to 6 h. Furthermore, drug accumulated in the skin after US treatment reached 158 $\mu g/cm^2$ after 6 hours.

4. Discussion

Vm currently represents the main stay against MRSA infections (Koyama et al., 2013; Kullar~~rrant~~ et al., 2016). However, Vm administration raises several issues that urgently need to be faced, including its marked instability, low oral bioavailability, complex concentration-time profile, low tissue penetration (ranging from 10% in diabetic to 30% in normal skin and soft tissues), and several adverse effects (Mawhinney et al., 1992; Raverdy et al., 2013; Vandecasteele et al., 2012; Vidal et al., 1992; Giandalia et al., 2001). In the attempt to counteract these drawbacks, thus improving the effectiveness of Vm delivery, some novel nanocarriers have been developed: i) Vm coupling to chitosan as an ocular drug delivery vehicle for topical use in rabbit eyes has appeared more effective than carrier-free Vm (Khangtragool et al., 2011); ii) PEGylated liposomal Vm enhanced the effective treatment of MRSA pneumonia and simultaneously reduced the nephrotoxicity risk compared with conventional and non-PEGylated Vm formulations (Muppidi et al., 2011); iii) Vm-loaded liposomes, stabilized with chitosan modified gold nanoparticles bounded to their surface, have proven effective in inhibiting the bacterial growth (Pornpattananangkul et al., 2011); and iv) Vm-containing trehalose and hydroxyethylcellulose spherical matrices have been developed as new delivery systems suitable for topical applications on extensive and purulent wounds (Giandalia et al., 2001). Recently, Vm-loaded polymersosomes were developed from a novel pegylated oleic acid polymer for sustained antibiotic delivery (Omolo et al., 2017). Overall, these works represent the proof-of-principle for the feasibility of choice of nanocarriers, as alternative drug delivery systems to obtain the desired drug release rates and bioavailability (Kalhapure et al., 2015). However, the effectiveness of those nanocarriers was seriously undermined by their poor ability to cross the *stratum corneum*, a skin barrier displaying low permeability unless proper exogenous physical stimuli are provided (Azagury et al., 2014; Park et al, 2012).

For these reasons, the present study aimed at developing Vm nanocarriers as a new platform to be effectively and safely employed for Vm topical administration to treat wound infections. To this purpose, NBs with core-shell nanostructures were identified as first choice carriers due to their known benefits in association with drug delivery, including small size, stability, suitability for drug loading, responsiveness to external stimuli such as US, and controlled drug release abilities (Marano et al., 2016; Cavalli et al., 2009a; Cavalli et al., 2009b; Cavalli et al., 2016). In this study, dextran sulfate was chosen as main constituent of the polysaccharidic shell as a consequence of the large amount of data from the literature supporting dextran biocompatibility (Bos et al., 2005; De Groot et al., 2001). Encouragingly, dextran-based hydrogels have already been employed as matrices in tissue engineering, without showing signs of inflammation *in vivo* (Möller et al., 2007), and recent toxicological studies have shown that dextran, as well as the products from its mechano-chemical processing, can be classified as class 4 (low-toxicity) substances (Dushkin et al., 2013). Moreover, dextran sulfate presents a negative charge that can electrostatically interact with the positive charged Vm. On the other hand, PFP was employed as principal constituent of the inner core, since it is the most widely used fluorocarbon in oxygenating emulsions and NB formulations (Cabrales and Intaglietta, 2013, Castro and Briceno, 2010). In order to load Vm, dextran sulfate-shelled/PFP-cored NBs were then functionalized by exploiting the electrostatic interactions occurring between the negatively charged sulfate groups of the shell and the protonated amino groups of the drug. The obtained VmLNBs displayed a spherical shape and a well-defined core-shell structure with a polymeric shell thickness of about 40 nm, average diameters of 300 nm, viscosity of 1.25 cP, and negatively charged surfaces. Of note, the observed decrease of zeta potential values of ~ 15 % for VmLNBs (around -29 mV) with respect to blank NBs (around -34 mV) confirmed the occurrence of electrostatic interactions between positive amino groups of the drug and negative sulfate groups of the polymer, leading to a partial

charge neutralization of the bubble surface and allowing a good Vm encapsulation efficiency (86%) and loading capacity (29%) in the NB systems.

In addition, it should be noticed that since the zeta potential measures charge repulsion or attraction between particles, it represents a fundamental parameter to avoid nanoparticle aggregation, with zeta potentials lower than -25 mV or larger than +25 mV being generally required for physical stability of colloid systems (Shah and Eldridge, 2014). The stability of VmLNB formulations was further confirmed by long-term checking of their size, surface charge, and viscosity values, which did not show any significant changes up to six months after manufacturing, stored at 4 °C. On the other hand, drug stability was comparatively checked between free Vm solution and VmLNB suspension either over time (up to 14 days) or at different temperatures (25°C and 37°C), revealing an increased stability for Vm when properly encapsulated in the nanocarriers. This appears as an undoubtedly advantageous feature for VmLNB formulations, since they might prove useful to overcome the reported instability of Vm in aqueous solutions at body temperature (Mawhinney et al., 1992, Raverdy ~~V~~ et al., 2013). Interestingly, VmLNBs displayed a slow and prolonged drug release kinetics compared to Vm aqueous solution, with only 16% of the drug being released from VmLNBs after 6 h. These data support the hypothesis that VmLNBs may be employed as an effective drug reservoir until reaching the target site, where the antibiotic would be released upon sonication at an appropriate moment only. The features of VmLNBs might be exploited for the design of innovative wound dressing following their inclusion in polymeric base. Indeed, NBs can be dispersed in polymer gel without changing physico-chemical characteristics, as previously showed (Prato et al., 2015). Another intriguing feature of VmLNBs relies on the reported evidence that surface charges play a pivotal role in making a nanoparticle suitable for topical treatment, since they enhance its interaction with the skin and improve its therapeutic effect on inflamed cutaneous tissues, either without (Abdel-Mottaleb et al., 2012) or with concomitant US treatment (Lopez et al., 2011). Although cationic nanoparticles are generally preferred for topical

506 treatment due to the anionic nature of the skin (Wu et al., 2010), some authors have shown that anionic
507 nanoparticles can be more effective (Lee et al., 2013) and less toxic (Ryman-Rasmussen et al., 2007)
508 than the cationic ones. These latter data appear consistent with our results through investigation by
509 biochemical assays to assess VmLNB biocompatibility with human skin tissues. Indeed, VmLNBs did
510 not induce any *in vitro* cytotoxic effects on HaCaT keratinocytes, a skin cell line that was originally
511 immortalized from a 62-year old donor (Boukamp et al., 1988). This peculiar information strengthens
512 remarkably the evidence on VmLNB safety for future topical applications.
513 VmLNB and carrier-free Vm antimicrobial activity against MRSA were comparatively investigated,
514 also analyzing Vm and NB physical interaction with the bacterial cell wall by confocal microscopy.
515 Interestingly, VmLNBs were more effective in MRSA bacterial growth inhibition then free Vm,
516 promoting enhanced and earlier antibacterial effects, although they were not internalized by bacteria,
517 opposite to free Vm. This behavior appears to be a likely consequence of time-sustained release of Vm
518 from VmLNBs.
519 Notably, an important issue that requires caution while evaluating the feasibility for any topical drug
520 treatment is represented by the considerably low degree of permeability of the skin, the primary
521 defense system for the body. This organ consists of several layers, including the *stratum corneum*, the
522 epidermis, and the dermis. In particular the *stratum corneum* - composed of corneocytes interspersed in
523 a laminate of compressed keratin and intercorneocyte lipid lamellae - is very poorly permeable to
524 foreign molecules and represents the main obstacle to transdermal drug delivery (Naik et al., 2000).
525 However, an ideal antibiotic drug formulation should be efficiently localized in the epidermis/dermis
526 and provide a sustained drug release over time (Prabhu et al., 2012). To allow a drug to penetrate the
527 skin, several approaches have been proposed, including skin patches, ionophoresis, chemical
528 enhancers, and US-triggered sonophoresis (Park et al., 2014).

Interestingly, antimicrobial properties have been reported for US, although its effectiveness strongly varies depending on the targeted type of pathogen (fungi vs bacteria; cocci vs bacilli; Gram-positive vs Gram-negative) (Sango et al., 2014). Furthermore, synergistic effects between US and antibiotics have been reported in a series of studies: i) antibiotic treatment coupled with US irradiation resulted in enhanced bactericidal activity against both Gram-positive and Gram-negative bacteria, especially for aminoglycosides (Yu et al., 2012); ii) the combination of Vm and US decreased *S. aureus* viable counts by two orders of magnitude compared to Vm alone (Ayan et al., 2008); and iii) the addition of NB-enhanced US to doxycycline treatment improved the drug effectiveness in eradicating intracellular *Chlamydia trachomatis* (Ikeka-Dantsuji et al., 2011). US-dependent enhancement of antibiotic action on biofilms was named as a 'bioacoustic effect'. Interestingly, Vm transfer through *S. epidermidis* biofilms was shown to be significantly enhanced by US, with bubbles being able to increase the biofilm permeability to Vm (Dong ~~Y.~~ et al., 2013).

As discussed previously, VmLNBs can be effectively employed as an important reservoir to store the drug until trespassing the *stratum corneum* of the skin and reaching the target site. In order to achieve the latter goal, US was assayed for its ability to induce VmLNBs to trespass an *in vitro* cutaneous layer, thereby releasing Vm throughout the skin. Notably, the skin from the pig ear is widely recognized as a good model for human skin permeability, since it displays human-like histological and physiological properties, including epidermal thickness and composition, dermal structure, lipid content and general morphology (Dick and Scott~~et al.~~, 1992). The validity of the porcine model has been established by comparing the permeability of simple marker molecules with the corresponding values across human skin (Herkenne et al., 2006, Sekkat et al., 2002). Therefore, the porcine ear skin represents so far the most accountable *in vitro* model to mimic the human skin in studies on percutaneous penetration (Jacobi et al., 2007). In our experiments, US appeared essential to promote Vm release from VmLNBs throughout the pig skin layers, in line with previous reports on NBs and sonophoresis. On the contrary,

the passive transport of free vancomycin hydrochloride was negligible, being a charged and hydrophilic molecule. The amount of Vm accumulated in the skin after US application combined with NBs was greater than MIC value.

5. Conclusions

In the present work, dextran sulfate-shelled and PFP~~perfluoropentane~~-filled NBs were developed for Vm delivery. VLNBs proved to be effective in MRSA bacterial killing without showing toxic effects on human keratinocytes. The combination of NBs and US enhanced Vm permeation through pig skin and promoted drug skin accumulation. Based on these results, Vm topical administration through proper NB formulations might be a promising strategy for the local treatment of MRSA skin infections. The study represents the proof of concept for the future development of advanced multifunctional therapeutic systems to treat infected wounds.

Acknowledgements

The present work was supported by funds from University of Torino (ex 60% to RC and RS), Compagnia di San Paolo (ORTO11CE8R 2011 to CG and Torino_call2014_L2_207 to AMC), and Fondazione Cariplo (HyWonNa project grant to MP). Thanks are due to Aurelio Malabaila for providing MRSA strain and to Giorgio Gribaudo for allowing to use his lab facilities to perform confocal microscopy studies.

.

References

Abdel-Mottaleb, M.M., Moulari, B., Beduneau, A., Pellequer, Y., Lamprecht, A., 2012. Surface-charge-dependent nanoparticles accumulation in inflamed skin. J. Pharm. Sci.101, 4231-4239.

Ayan, İ., Aslan, G., Çömelekoğlu, Ü., Yılmaz, N., Çolak, M., 2008. The effect of low-intensity pulsed sound waves delivered by the Exogen device on Staphylococcus aureus morphology and genetics. Acta orthop. ~~aedica et~~ traumatol. ~~ogica~~ turc. ~~ica~~ 42(4), 272-277.

Azagury, A., Khoury, L., Enden, G., Kost, J., 2014. Ultrasound mediated transdermal drug delivery. Adv. drug del. rev. 72, 127-143.

Banche, G., Prato, M., Magnetto, C., Allizond, V., Giribaldi, G., Argenziano, M., Khadjavi, A., Gulino, G.R., Finesso, N., Mandras, N., Tullio, V., Cavalli, R., Guiot, C., Cuffini, A.M., -2015. Antimicrobial chitosan nanodroplets: new insights for ultrasound-mediated adjuvant treatment of skin infection. Future Microbiol. 10(6), 929-939. doi: 10.2217/fmb.15.27. PubMed PMID: 26059617.

Basilico, N., Magnetto, C., D'Alessandro, S., Panariti, A., Rivolta, I., Genova, T., Khadjavi, A., Gulino, G.R., Argenziano, M., Soster, M., Cavalli, R., Giribaldi, G., Guiot, C., Prato, M., 2015. Dextran-shelled oxygen-loaded nanodroplets reestablish a normoxia-like pro-angiogenic phenotype and behavior in hypoxic human dermal microvascular endothelium. Toxicol. Appl. Pharmacol. 288(3), 330-338. doi: 10.1016/j.taap.2015.08.005. Epub 2015 Aug 12. PubMed PMID: 26276311.

598 Bos, G.W., Hennink, W.E., Brouwer, L.A., den Otter, W., Veldhius, F.J., van Nostrum, C.F., van Luyn
599 M.J., 2005. Tissue reactions of in situ formed dextran hydrogels crosslinked by stereocomplex
600 formation after subcutaneous implantation in rats. Biomaterials 26, 3901–3909.
601
602 Boukamp, P., Dzarlieva-Petrusevska, R.T., Breitkreuz, D., Hornung, J., Markham, A., Fusenig, N.E.,
603 1988. Normal keratinization in a spontaneously immortalized aneuploid human keratinocyte cell line. J.
604 Cell. Biol. 106, 761-771.
605
606 Cabrales, P., Intaglietta, M., 2013. Blood substitutes: evolution from noncarrying to oxygen- and gas-
607 carrying fluids. ASAIO J. 59, 337-354.
608
609 Castro, C.I., Briceno, J.C., 2010. Perfluorocarbon-based oxygen carriers: review of products and trials.
610 Artif. Organs. 34, 622-634.
611
612 Cavalli, R., Bisazza, A., Rolfo, A., Balbis, S., Madonnaripa, D., Caniggia, I., Guiot, C., 2009a.
613 Ultrasound-mediated oxygen delivery from chitosan nanobubbles. Int. J. Pharm. 378, 215–217.
614
615 Cavalli, R., Bisazza, A., Giustetto, P., Civra, A., Lembo, D., Trotta, G., Guiot, C., Trotta, M., 2009b.
616 Preparation and characterization of dextran nanobubbles for oxygen delivery. Int. J. Pharm. 381, 160-
617 165.
618
619 Cavalli, R., Bisazza, A., Trotta, M., Argenziano, M., Civra, A., Donalisio, M., Lembo, D., 2012. New
620 chitosan nanobubbles for ultrasound-mediated gene delivery: preparation and in vitro characterization.
621 Int. J. Nanomed. 7, 3309-3318.

Cavalli, R., Bisazza, A., Lembo, D., 2013. Micro-and nanobubbles: A versatile non-viral platform for gene delivery. Int. J. Pharm. 456(2), 437-445.

Cavalli, R., Soster, M., Argenziano, M., 2016. Nanobubbles: a promising efficienft tool for therapeutic delivery. Ther. Deliv. 7(2), 117-138. doi: 10.4155/tde.15.92. Epub 2016 Jan 15. PubMed PMID: 26769397.

Clinical and Laboratory Standards Institute. Performance standards for antimicrobial susceptibility testing. Twenty-second informational supplement. Document M100-S22. Vol . 32, No. 3. Wayne, PA: CLSI; 2012.

Cumming, G., Fidler, F., Vaux, D.L., 2007. Error bars in experimental biology. J Cell Biol. 177, 7-11.

Daeschlein, G., 2013. Antimicrobial and antiseptic strategies in wound management. Int. Wound J. 10(1), 9-14. doi: 10.1111/iwj.12175. Review. PubMed PMID:24251838.

De Groot C.J., Van Luyn, M.J.A., Van DijK-Wolthuis, Cadée, J.A., Plantinga, J.A., Den Otter, W., Hennink, W.E., 2001. In vitro biocompatibility of biodegradable dextran-based hydrogels tested with human fibroblast. Biomaterials 22, 1197–1203.

Delalande, A., Postema, M., Mignet, N., Midoux, P., Pichon, C., 2012. Ultrasound and microbubble-assisted gene delivery: recent advances and ongoing challenges. Ther. Deliv. 3, 1199-1215.

Dick, I.P., Scott, R.C. 1992. Pig ear skin as an in-vitro model for human skin permeability. J. Pharm. Pharmacol. 44, 640–645.

Diehr, P., O'Meara, E.S., Fitzpatrick, A., Newman, A.B., Kuller, L., Burke, G., 2008. Weight, mortality, years of healthy life, and active life expectancy in older adults. J. Am. Geriatr. Soc. 56(1), 76-83. Epub 2007 Nov 20. PubMed PMID: 18031486; PubMed Central PMCID: PMC3865852.

Dong, Y., Chen, S., Wang, Z., Peng, N., Yu, J., 2013. Synergy of ultrasound microbubbles and vancomycin against Staphylococcus epidermidis biofilm. J. Antimicrob.~~ial~~ Chemother.~~apy~~ 68, 816-826.

Dushkin, A.V., Meteleva, E.S., Tolstikova, T.G., Pavlova, A.V., Khvostov, M.V. 2013. Gel chromatographic and toxicological studies of the mechanochemical transformations of water-soluble polysaccharides. Pharm. Chem. J. 46, 630-633.

Fokong, S., Theek, B., Wu, Z., Koczera, P., Appold, L., Jorge, S., Resch-Genger, U., VanZandvoort, M., Storm, G., Kiessling, F., Lammers, T., 2012. Image-guided, targeted and triggered drug delivery to tumors using polymer-based microbubbles. J. Control. Rel. 163, 75–81.

Giandalia, G., De Caro, V., Cordone, L., Giannola, L.I. 2001. Trehalose-hydroxyethylcellulose microspheres containing vancomycin for topical drug delivery. Eur. J. Pharm. and Biopharm.: official journal of Arbeitsgemeinschaft fur Pharmazeutische Verfahrenstechnik e.V. 52, 83-89.

669 Guiot, C., Pastore, G., Napoleone, M., Gabriele, P., Trotta, M., Cavalli, R., 2006. Thermal response of
670 contrast agent microbubbles: preliminary results from physico-chemical and US-imaging
671 characterization. Ultrasonics. 44(1), 127-130. Epub 2006 Jun 30. PubMed PMID: 17056082.
672
673 Gulino, G.R., Magnetto, C., Khadjavi, A., Panariti, A., Rivolta, I., Soster, M., Argenziano, M., Cavalli,
674 R., Giribaldi, G., Guiot, C., Prato, M., 2015. Oxygen-Loaded Nanodroplets Effectively Abrogate
675 Hypoxia Dysregulating Effects on Secretion of MMP-9 and TIMP-1 by Human Monocytes. Mediators
676 Inflamm. 2015, 964838. doi: 10.1155/2015/964838. Epub 2015 Mar 23. PubMed PMID: 25878404;
677 PubMed Central PMCID: PMC4386605.
678
679 Gurusamy, K.S., Koti, R., Toon, C.D., Wilson, P., Davidson, B.R., 2013. Antibiotic therapy for the
680 treatment of methicillin-resistant Staphylococcus aureus (MRSA) infections in surgical wounds.
681 Cochrane Database Syst. Rev. 20, 8:CD009726. doi: 10.1002/14651858.CD009726.pub2. Review.
682 PubMed PMID: 23963687.
683
684 Herkenne, C., Naik, A., Kalia, Y.N., Hadgraft, J., Guy, R.H., 2006. Pig ear skin ex vivo as a
685 model for in vivo dermatopharmacokinetic studies in man. Pharm. Res. 23, 1850-1856.
686
687 Ikeda-Dantsuji, Y., Feril, L. B., Tachibana, K., Ogawa, K., Endo, H., Harada, Y., Suzuki, R.,
688 Maruyama, K., 2011. Synergistic effect of ultrasound and antibiotics against Chlamydia trachomatis-
689 infected human epithelial cells in vitro. Ultrason.~~ics~~ sonochem.~~istry~~ 18(1), 425-430.
690
691 Jacobi, U., Kaiser, M., Toll, R., Mangelsdorf, S., Audring, H., Otberg, N., Sterry, W., Lademann, J.,
692 2007. Porcine ear skin: an in vitro model for human skin. Skin Research and Technology 13(1), 19–24.

Karshafian, R., Bevan, P.D., Williams, R., Samac, S., Burns, P.N., 2009. Sonoporation by ultrasound-activated microbubble contrast agents: effect of acoustic exposure parameters on cell membrane permeability and cell viability. Ultrasound Med. Biol. 35, 847-860.

Khadjavi, A., Magnetto, C., Panariti, A., Argenziano, M., Gulino, G.R., Rivolta, I., Cavalli, R., Giribaldi, G., Guiot, C., Prato, M., 2015. Chitosan-shelled oxygen-loaded nanodroplets abrogate hypoxia dysregulation of human keratinocyte gelatinases and inhibitors: New insights for chronic wound healing. Toxicol. Appl. Pharmacol. 286(3), 198-206. doi: 10.1016/j.taap.2015.04.015. Epub 2015 Apr 30. PubMed PMID: 25937238.

Kalhapure, R.S., Suleman, N., Mocktar, C., Seedat, N., Govender, T., 2015. Nanoengineered Drug Delivery Systems for Enhancing Antibiotic Therapy. J. Pharm. Sci. 104, 872–905.

Khangtragool, A., Ausayakhun, S., Leesawat, P., Laokul, C., Molloy, R., 2011. Chitosan as an ocular drug delivery vehicle for vancomycin. J. App. Pol. Sci. 122, 3160-3167.

Koyama, N., Inokoshi, J., Tomoda, H., 2012. Anti-infectious agents against MRSA. Molecules 18(1), 204-224. doi: 10.3390/molecules18010204.

Kullar, R., Sakoulas, G., Deresinski, S., van Hal, S. J., 201~~6~~5. When sepsis persists: a review of MRSA bacteraemia salvage therapy. J. Antimicrob. Chemother. 71, 576-586.

Formatted: English (United States)

Formatted: English (United States)

Formatted: English (United States)

716 Lazarus, G.S., Cooper, D.M., Knighton, D.R., Percoraro, R.E., Rodeheaver, G., Robson, M.C., 1994.
717 Definitions and guidelines for assessment of wounds and evaluation of healing. Wound Repair Regen.
718 2(3), 165-170. PubMed PMID: 17156107.
719
720 Lee, O., Jeong, S.H., Shin, W.U., Lee, G., Oh, C., Son, S.W., 2013. Influence of surface charge of gold
721 nanorods on skin penetration. Skin Res. Technol. 19, e390-e396.
722
723 Lopez, R.F., Seto, J.E., Blankschtein, D., Langer, R., 2011. Enhancing the transdermal delivery of rigid
724 nanoparticles using the simultaneous application of ultrasound and sodium lauryl sulfate. Biomaterials.
725 32, 933-941.
726
727 Magnetto, C., Prato, M., Khadjavi, A., Giribaldi, G., Fenoglio, I., Jose, J., Gulino, G.R., Cavallo, F.,
728 Quaglino, E., Benintende, E., Varetto, G., Troia, A., Cavalli, R., Guiot, C., 2014. Ultrasound-activated
729 decafluoropentane-cored and chitosan-shelled nanodroplets for oxygen delivery to hypoxic cutaneous
730 tissues. RSC Advances 4, 38433-38441.
731
732 Marano, F., Argenziano, M., Frairia, R., Adamini, A., Bosco, O., Rinella, L., Fortunati, N., Cavalli, R.,
733 Catalano, M.G., 2016. Doxorubicin-Loaded Nanobubbles Combined with Extracorporeal Shock
734 Waves: Basis for a New Drug Delivery Tool in Anaplastic Thyroid Cancer. Thyroid 26(5), 705-716
735
736 Markova. A., Mostow, E.N., 2012. US skin disease assessment: ulcer and wound care. Dermatol. Clin.
737 30(1), 107-111. ix. doi: 10.1016/j.det.2011.08.005. Review. PubMed PMID: 22117872.
738

739 Marxer, E.E.J., Brüßler, J., Becker, A., Schümmelfeder, J., Schubert, R., Nimsky, C., Bakowsky, U.,
740 2011. Development and characterization of new nanoscaled ultrasound active lipid dispersions as
741 contrast agents. Eur. J. Pharm. Biopharm. 77, 430–437.
742
743 Mawhinney, W.M., Adair, C.G., Gorman, S.P., McClurg, B., 1992. Stability of vancomycin
744 hydrochloride in peritoneal dialysis solution. Am. J. Hosp. Pharm. 49(1), 137-139. PubMed PMID:
745 1570857.
746
747 Möller, S., Weisser, J., Bischoff, S., Schnabelrauch, M., 2007. Dextran and hyaluronan methacrilate
748 based hydrogels as matrices for soft tissue reconstruction. Biomol. Eng. 24, 496–504.
749
750 Muppidi, K., Wang, J., Betageri, G., Pumerantz, A.S. 2011. PEGylated liposome encapsulation
751 increases the lung tissue concentration of vancomycin. Antimicrob. Agents Chemother. 55(10), 4537-
752 4542.
753
754 Naik, A., Kalia, Y.N., Guy, R.H., 2000. Transdermal drug delivery: overcoming the skin's barrier
755 function. Pharm. Sci. Technol. Today. 3, 318–326.
756
757 Omolo, C.A., Kalhapure, R.S., Jadhav, M., Rambharose, S., Mocktar, C., Ndesendo, V.M., Govender,
758 T. 2017. PEGylated oleic acid: A promising amphiphilic polymer for nano-antibiotic delivery. Eur. J.
759 Pharm. Biopharm. 112, 96-108.
760

761 Park, D., Ryu, H., Kim, H.S., Kim, Y.S., Choi, K.S., Park, H., Seo J., 2012. Sonophoresis Using
762 Ultrasound Contrast Agents for Transdermal Drug Delivery: An In Vivo Experimental Study.
763 Ultrasound Med. & Biol. 38(4), 642-650.
764
765 Park, D., Park, H., Seo, J., Lee, S., 2014. Sonophoresis in transdermal drug delivery. Ultrasonics. 54,
766 56-65.
767
768 Payne, W.G., Naidu, D.K., Wheeler, C.K., Barkoe, D., Mentis, M., Salas, R.E., Smith, D.J., Robson,
769 M.C., 2008. Wound healing in patients with cancer. Eplasty. 8, e9. PubMed PMID: 18264518; PubMed
770 Central PMCID: PMC2206003.
771
772 Pornpattananangkul, D., Zhang, L., Olson, S., Aryal, S., Obonyo, M., Vecchio, K., Huang, C.M.,
773 Zhang, L., 2011. Bacterial toxin-triggered drug release from gold nanoparticle-stabilized liposomes for
774 the treatment of bacterial infection. J. American Chem. Soc.133(11), 4132-4139.
775
776 Prabhu, P., Patravale, V., Joshi, M., 2012. Nanocarriers for effective topical delivery of anti-infectives.
777 Current Nanoscience 8, 491-503.
778
779 Prato, M., Magnetto, C., Jose, J., Khadjavi, A., Cavallo, F., Quaglino, E., Panariti, A., Rivolta, I.,
780 Benintende, E., Varetto, G., Argenziano, M., Troia, A., Cavalli, R., Guiot C., 2015. 2H,3H-
781 decafluoropentane-based nanodroplets: new perspectives for oxygen delivery to hypoxic cutaneous
782 tissues. Plos One 10(3), e0119769. doi:10.1371/journal.pone.0119769
783

784 Prato, M., Khadjavi, A., Magnetto, C., Gulino, G.R., Rolfo, A., Todros, T., Cavalli, R., Guiot, C., 2016.
785 Effects of oxygen tension and dextran-shelled/2H,3H-decafluoropentane-cored oxygen-loaded
786 nanodroplets on secretion of gelatinases and their inhibitors in term human placenta. Biosci Biotechnol
787 Biochem. 80(3), 466-472. doi: 10.1080/09168451.2015.1095068. Epub 2015 Nov 2. PubMed PMID:
788 26523859.
789
790 Price, M., 2010. Community-acquired methicillin-resistant Staphylococcus aureus: an ongoing
791 challenge for WOC nursing. J Wound Ostomy Continence Nurs. 37(6), 633-638. doi:
792 10.1097/WON.0b013e3181feb001. Review. PubMed PMID: 21076263.
793
794 Raverdy V., Ampe, E., Hecq, J.D., Tulkens, P. M., 2013. Stability and compatibility of vancomycin for
795 administration by continuous infusion. J. Antimicrob. Chemother. 68, 1179-1182.
796
797 Ryman-Rasmussen, J.P., Riviere, J.E., Monteiro-Riviere, N.A., 2007. Surface coatings determine
798 cytotoxicity and irritation potential of quantum dot nanoparticles in epidermal keratinocytes. J Invest
799 Dermatol. 127, 143-153.
800
801 Sango, D.M., Abela, D., McElhatton, A., Valdramidis, V.P., 2014. Assisted ultrasound applications for
802 the production of safe foods. J. Appl. Microbiol. 116, 1067-1083.
803
804 Sekkat, N., Kalia, Y.N., Guy, R.H., 2002. Biophysical study of porcine ear skin in vitro and its
805 comparison to human skin in vivo. J. Pharm. Sci. 91, 2376-2381.
806 Shah, R., Eldridge, R., 2014. Optimisation and Stability Assessment of Solid Lipid Nanoparticles using
807 Particle Size and Zeta Potential. J. Phys. Sci, 25, 59–75

Sharma, A., Arya, D.K., Dua, M., Chhatwal, G.S., Johri, A.K., 2012. Nano-technology for targeted drug delivery to combat antibiotic resistance. Expert Opinion Drug Del. 9, 1325-1332.

Vandecasteele, S.J., De Vriese, A.S., Tacconelli, E., 2012. The pharmacokinetics and pharmacodynamics of vancomycin in clinical practice: evidence and uncertainties. J. Antim. Chem. 68, 743-748.

Vidal, C., González Quintela, A., Fuente, R., 1992. Toxic epidermal necrolysis due to vancomycin. Ann Allergy. 68(4), 345-347. PubMed PMID: 1558331.

Wu, X., Landfester, K., Musyanovych, A., Guy, R.H., 2010. Disposition of charged nanoparticles after their topical application to the skin. Skin Pharmacol Physiol. 23, 117-123.

Yin, T., Wang, P., Li, J., Wang, Y., Zheng, B., Zheng, R., Cheng, D., Shuai, X., 2014. Tumor-penetrating codelivery of siRNA and paclitaxel with ultrasound-responsive nanobubbles hetero-assembled from polymeric micelles and liposomes. Biomaterials 35(22), 5932-5943.

Yu, H., Chen, S., Cao, P., 2012. Synergistic bactericidal effects and mechanisms of low intensity ultrasound and antibiotics against bacteria: a review. Ultrasonics sonochemistry 19(3), 377-382.

Zilberman, M., Elsner, J.J., 2008. Antibiotic-eluting medical devices for various applications. J Control Release 130(3), 202-215. doi: 10.1016/j.jconrel.2008.05.020. Epub 2008 Aug 6. Review. PubMed PMID: 18687500.

Figure legends

Figure 1. **Schematic structure of VmLNB formulations.** Vm nanocarriers described in the present work display a core-shell structure. PFP was employed as core fluorocarbon, whereas dextran sulfate was chosen as polysaccharidic shell molecule. Vm was inserted into the outer shell throughout dextran sulfate chains. In selected experiments, VmLNBs were further functionalized by including fluorescent 6-coumarin in the inner core.

Figure 2. NB and VmLNB morphology. NBs and VmLNBs were checked for morphology by TEM. Results are shown as representative images from three different preparations. Panel A. NB image by TEM. Panel B. VmLNB image by TEM. (see also Figure S1 in Supplementary Materials for additional images of multiple nanobubbles within the same field).

Figure 3. Stability of Vm and VmLNB formulations. The stability of Vm solution and VmLNB suspension was monitored up to 14 days either at room temperature (Panel A) or at 37°C (Panel B) through analysis by HPLC. Results are shown as means ± SD from three different preparations for each formulation. Data were also analyzed for significance by ANOVA. Versus Vm solution: * $p<0.001$.

Figure 4. Biocompatibility of Vm and VmLNBs with human keratinocytes *in vitro*. HaCaT cells (10^6 cells/2 mL DMEM medium implemented with 10% FCS) were left untreated (ctr) or treated with 200 ~~micro~~μL of Vm solution or VmLNB suspension for 24 h in normoxia (20% O_2). Thereafter, Vm and VmLNB cytotoxicity were measured through LDH assay (Panel A), whereas cell viability was measured through MTT assay (Panel B). Results are shown as means ± SEM from three independent

experiments. Data were also evaluated for significance by ANOVA. No significant differences were found among all conditions.

Figure 5. *In vitro* Vm release from Vm and VmLNB formulations. Vm release from Vm solution and VmLNB suspension was monitored up to 6 h. Results are shown as means ± SD from three different preparations for each formulation. Data were also analyzed for significance by ANOVA. Versus Vm solution: * $p<0.001$.

Figure 6. Antibacterial activity of Vm and VmLNBs against MRSA. MRSA were left for 2, 3, 4, 6 and 24 hours at 37°C alone (ctr) or incubated with 10% v/v NBs or different concentrations of Vm, either free or loaded on VmLNBs (Panel A: 1 mg/mL; Panel B: 0.1 mg/mL; Panel C: 0.01 mg/mL; Panel D: 0.004 mg/mL). Results are shown as means ± SEM from three independent experiments. Data on Vm- and VmLNB-treated samples were normalized upon Vm/VmLNB release ratios reported in Table 2~~3~~ (see also in Supplementary Materials: Table S3~~1~~ for further information on percentages of drug release from VmLNBs at different times/concentrations; and Figure S2~~1~~ for raw data on VmLNB antibacterial effects). All data were also evaluated for significance by ANOVA. Versus ctr: * $p < 0.02$; versus Vm: ° $p < 0.05$.

Figure 7. Drug loading on dextran sulfate-shelled NBs prevents Vm internalization by MRSA. MRSA were left alone or incubated with 10% v/v 6-coumarin-labeled VLNBs, 6-coumarin-labeled NBs, and FITC-labeled Vm for 2h at 37°C. After staining bacteria with PI, confocal fluorescent images were taken using FITC and TRITC filters. Data are shown as representative images from three independent experiments. Magnification: 100X. Red: PI. Green: 6-coumarin or FITC.

878 **Figure 8. US-triggered sonophoresis of VmLNBs through skin membranes.** US (t = 10 min; f = 2.5
879 MHz; P = 5 W) abilities to induce sonophoresis and Vm permeation from VmLNBs were evaluated up
880 to 6 h by using a vertical diffusion Franz cell consisting in two chambers (donor and recipient,
881 respectively) separated by a pig skin layer (see scheme in Panel A). Results are shown in Panel B as
882 means ± SD from three independent experiments. Data were also evaluated for significance by
883 ANOVA. Versus without US: $p < 0.001$.

Tables and legends

Formulation	Average diameter ± SD (nm)	Polydispersity index	Zeta Potential ± SD (mV)	Viscosity (cP)
NBs	313.4 ± 26.4	0.24 ± 0.02	- 34.5 ± 0.38	1.22
VmLNBs	304.6 ± 14.6	0.22 ± 0.03	- 28.6 ± 1.34	1.25
Fluorescent NBs	312.8 ± 22.7	0.25 ± 0.02	- 34.1 ± 1.22	1.24
Fluorescent VmLNBs	308.9 ± 22.4	0.23 ± 0.01	- 29.5 ± 1.88	1.23

Formatted Table

Table 1. Physical-chemical characterization of NB~~b~~s and VmLNBs. Liquid formulations were characterized for average diameters, polydispersity index, and zeta potential by light scattering. The viscosity (cP) of NB and VmLNB suspensions was determined at 25 °C by using a Ubbelohde capillary viscosimeter. Results are shown as means ± SD from three preparations. See also Figures 1-2 for further detail on NB and VmLNB structure and morphology.

~~Sample solution~~ ~~Viscosity (cP)~~

~~Vm~~ ~~0.98~~

~~NBs~~ ~~1.12~~

~~VmLNBs~~ ~~1.25~~

~~**Table 2. Viscosity of Vm solution, NB, and VmLNB suspensions.** The viscosity (cP) of NB and VmLNB suspensions as well as free Vm solution was determined at 25 °C by using a Ubbelohde capillary viscosimeter. The results are reported in the table.~~

time (hours)	% drug release from Vm solution	% drug release from VmLNBs	Vm/VmLNB drug release ratio
2	36.57	5.99	6.11
3	45.97	7.97	5.78
4	57.16	10.27	5.57
6	73.44	14.59	5.03
24	92.34	35.84	2.58

Table 2~~3~~. *In vitro* drug release from Vm solution and VmLNB suspension. After incubation for increasing times (first column), the percentages of *in vitro* drug release from Vm solution (second column) and VmLNB suspension (third column) were measured. Then, Vm/VmLNB drug release ratios (fourth column) were calculated for each time considered. All incubation times (2, 3, 4, 6, and 24 h) were purposely chosen to further normalize the results from the experiments with MRSA (see Figure 6). Results are shown as mean values from three different preparations for each formulation.

Figure 1

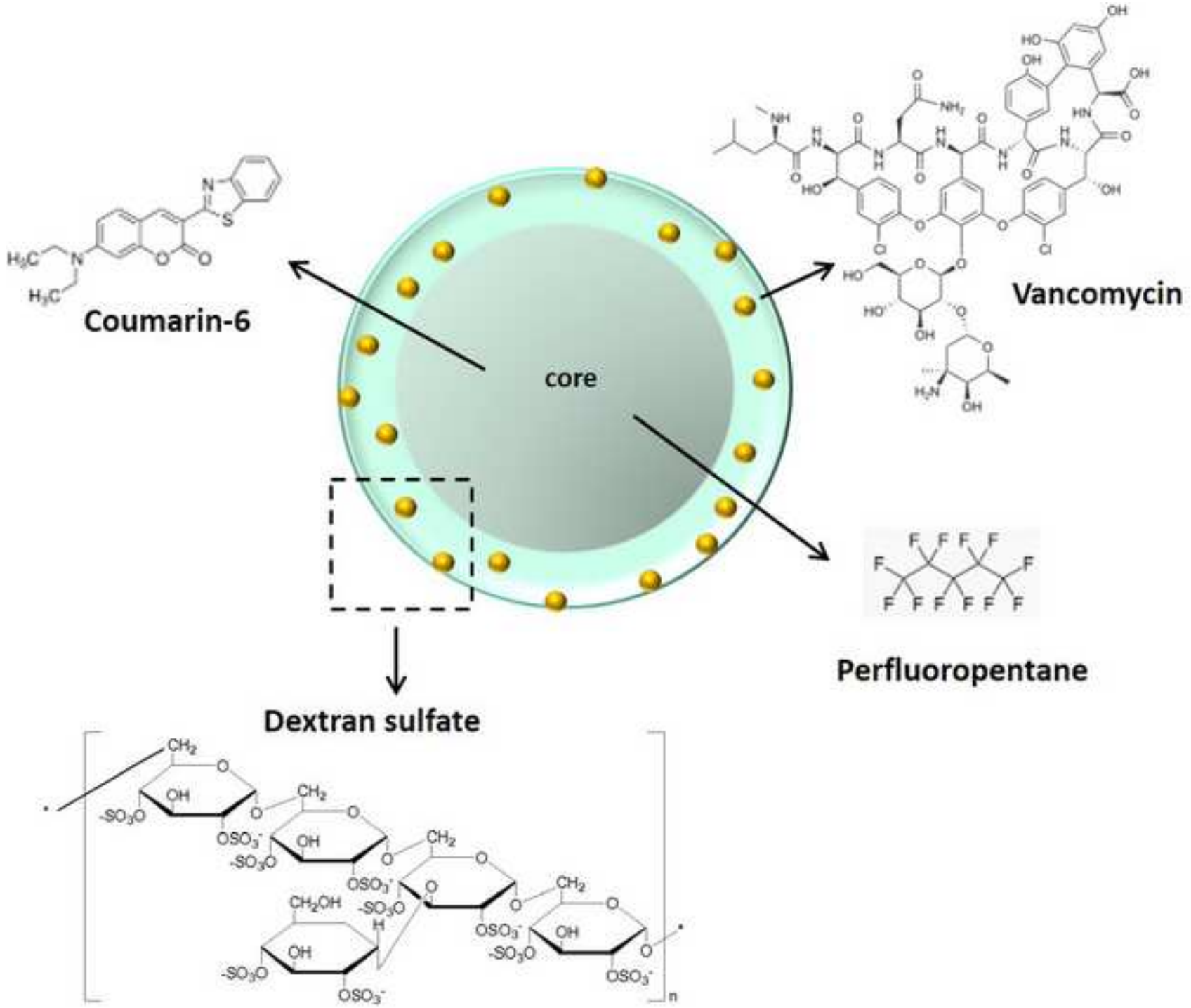
Coumarin-6
Vancomycin
core
Perfluoropentane
Dextran sulfate

Figure 2

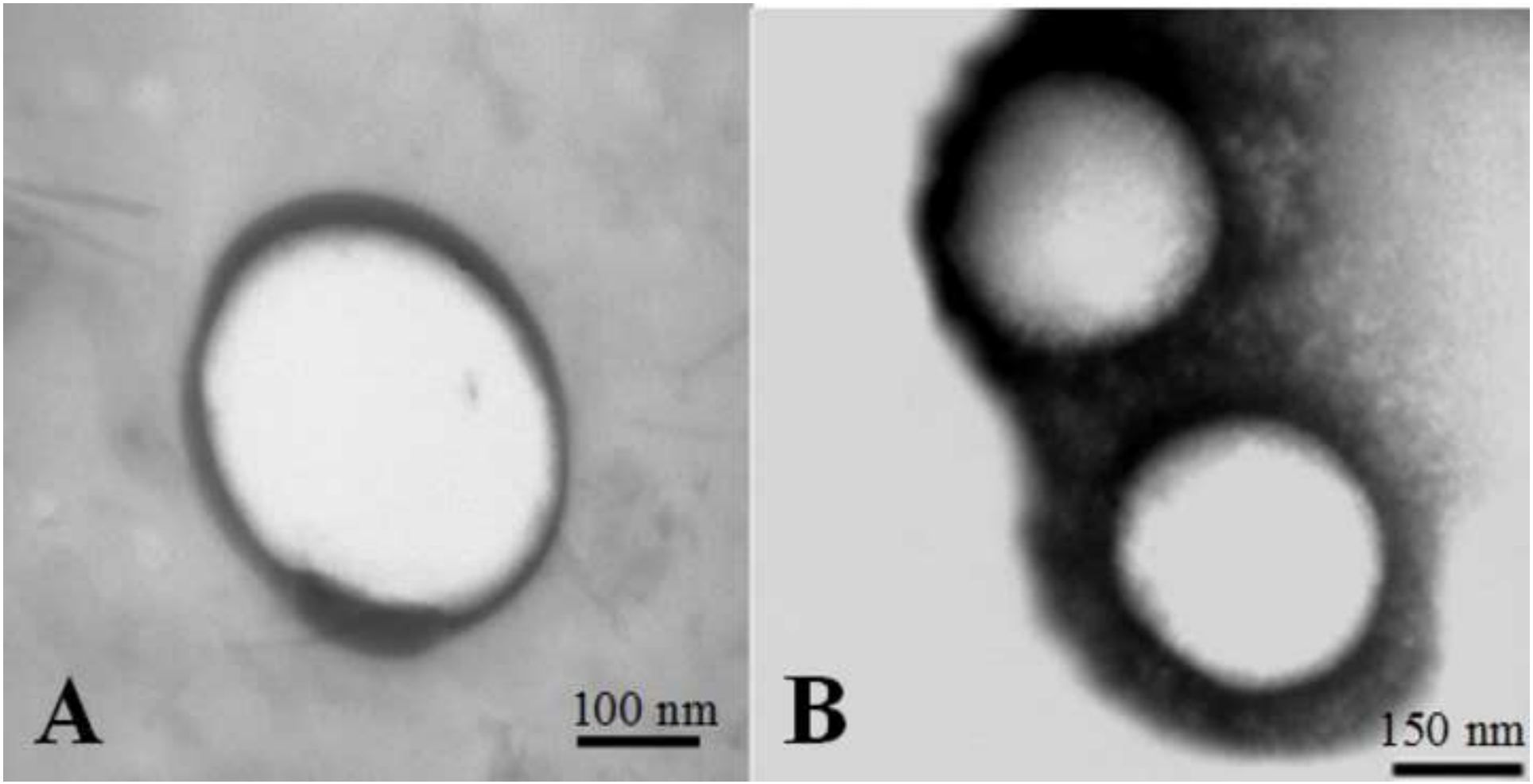

Figure 3

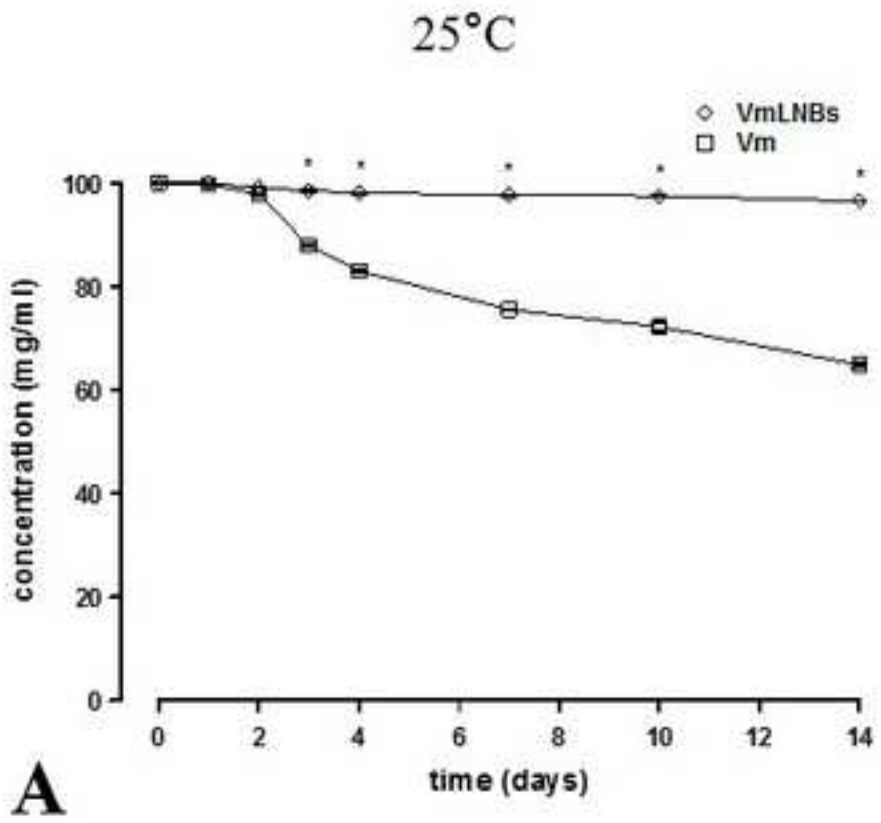
25°C
VmLNBs
Vm
concentration (mg/ml)
time (days)
A

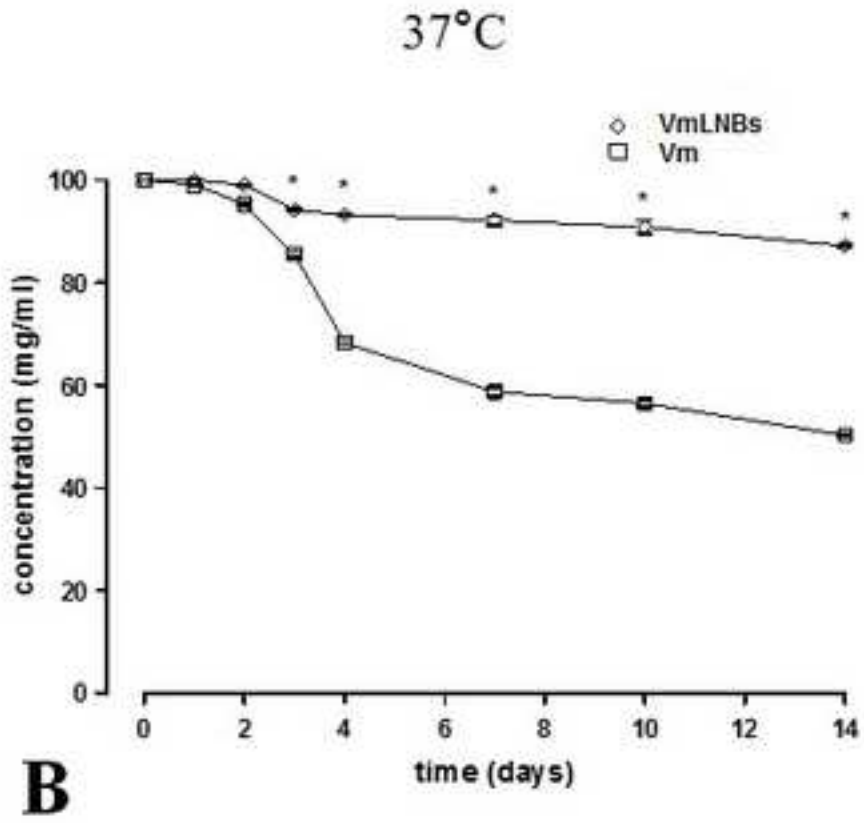
37°C
VmLNBs
Vm
concentration (mg/ml)
time (days)
B

Figure 4

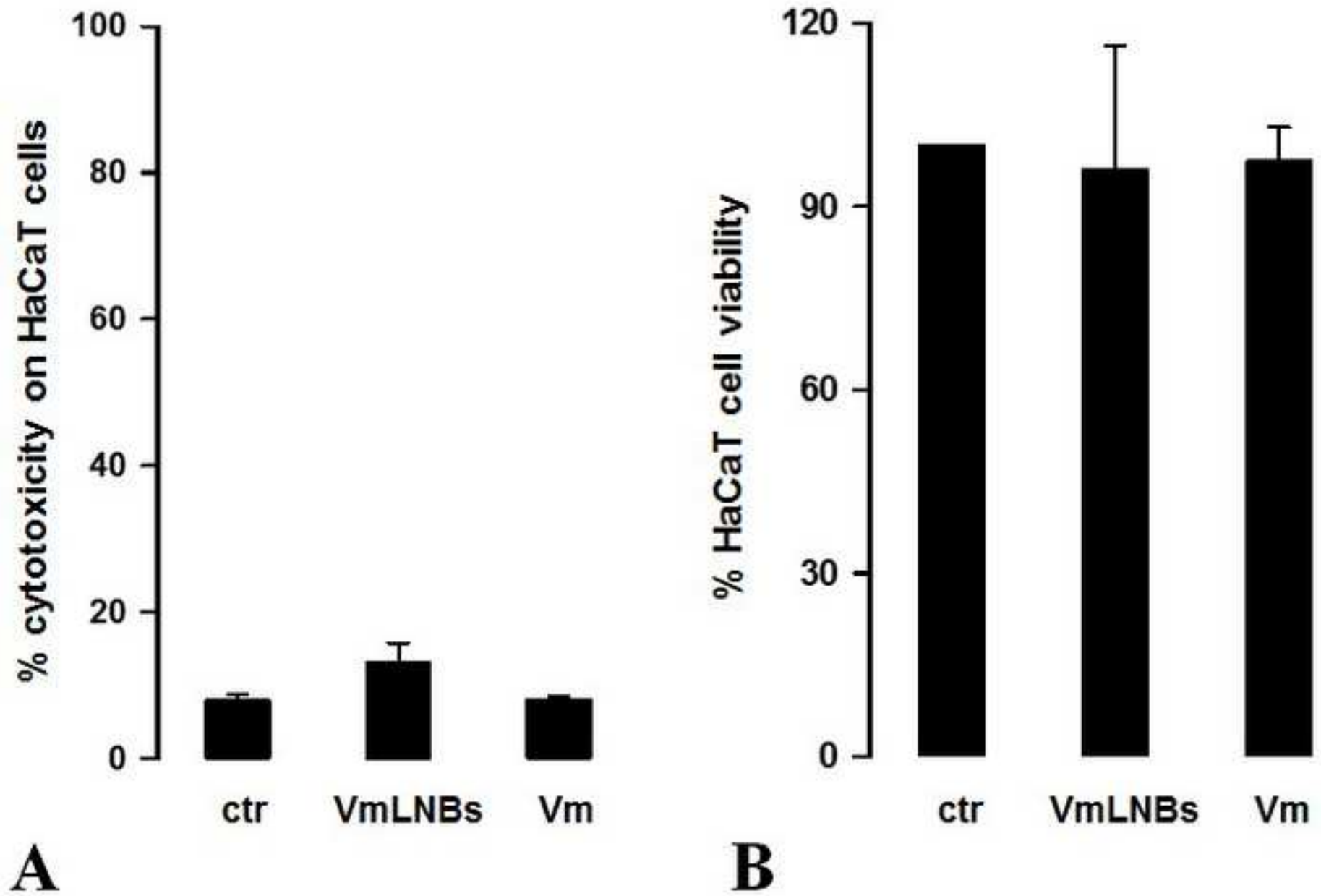
% cytotoxicity on HaCaT cells
100
80
60
40
20
0
ctr
VmLNBs
Vm
A
% HaCaT cell viability
120
90
60
30
0
ctr
VmLNBs
Vm
B

Figure 5

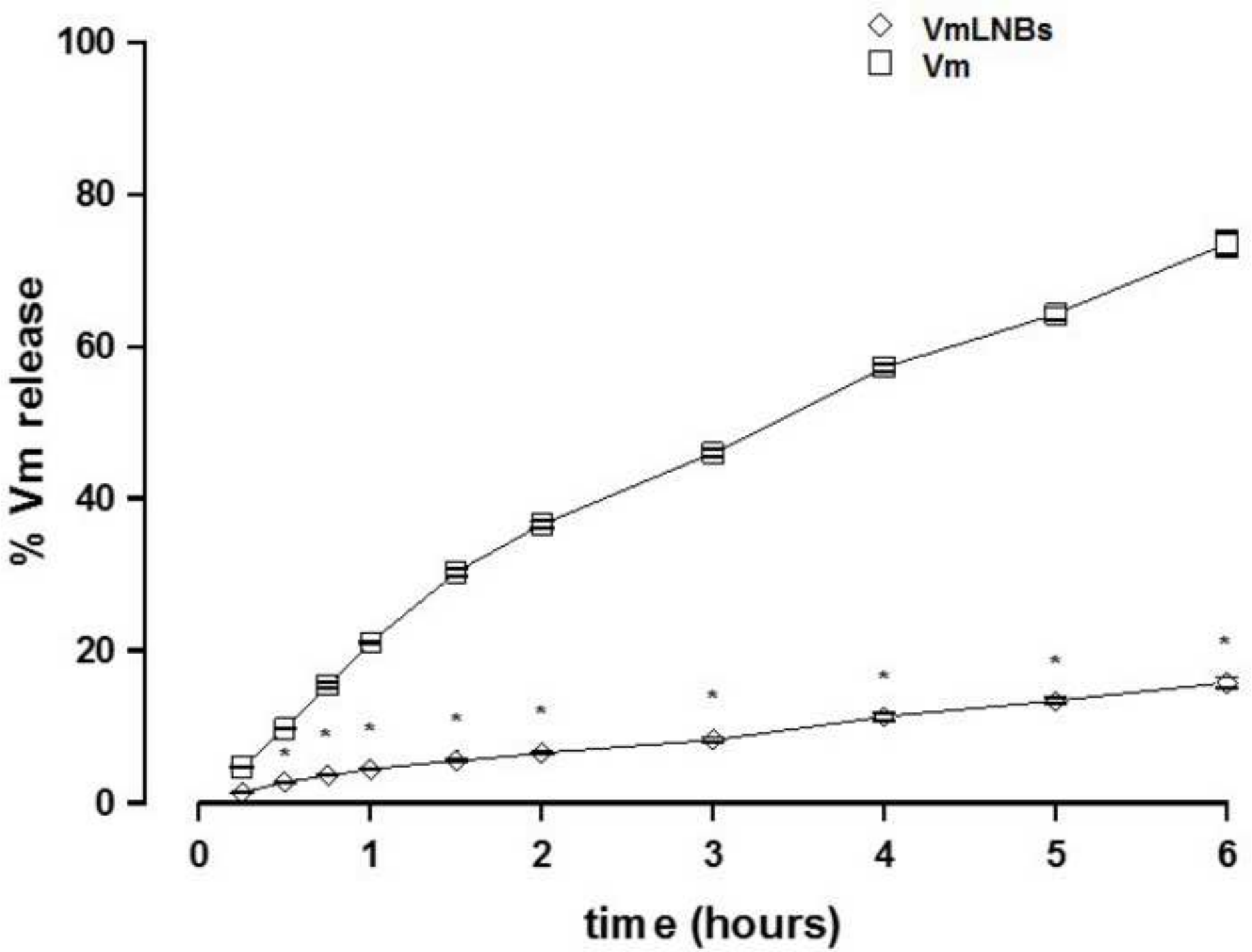

Figure 6

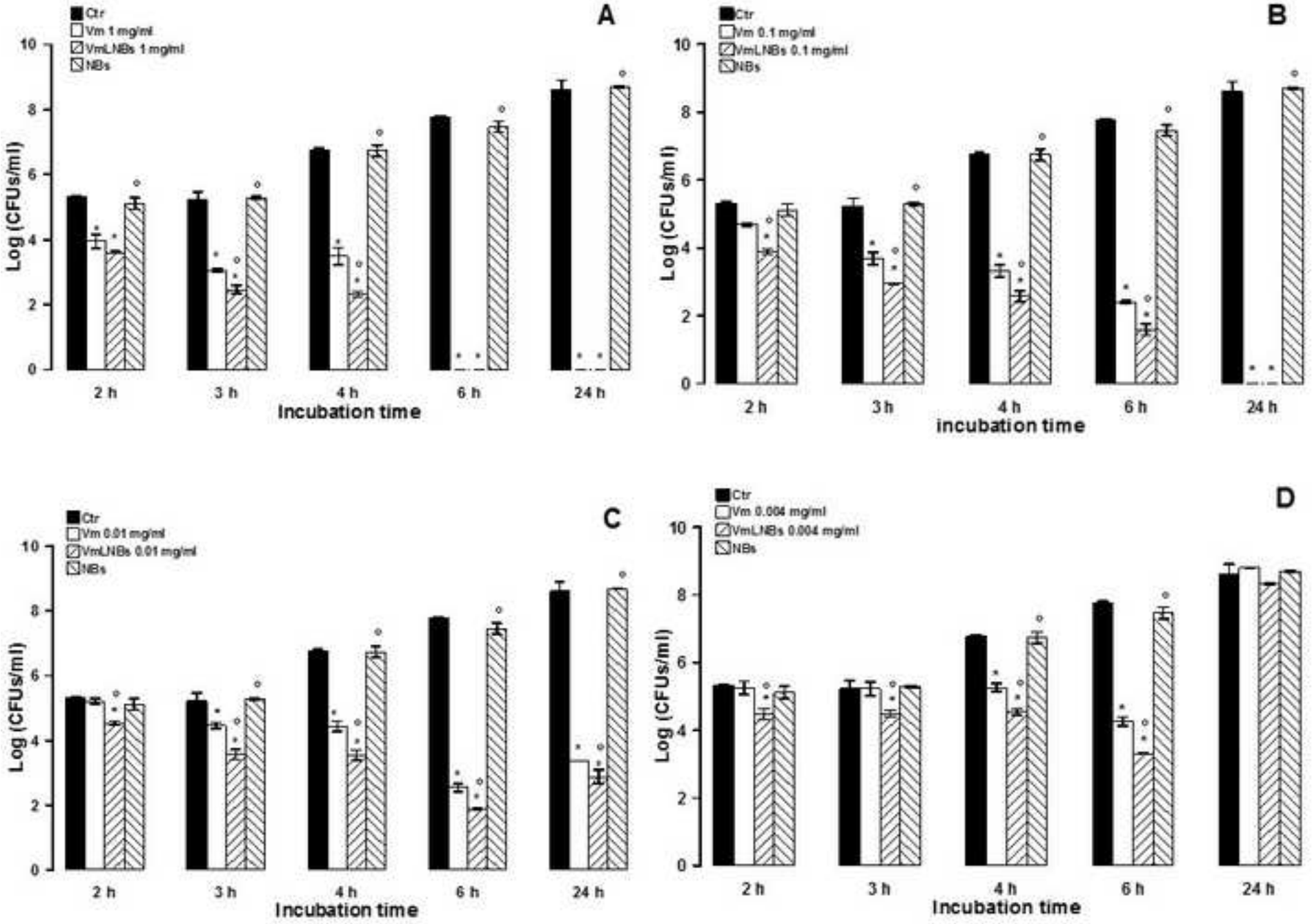
A
Ctr
Vm 1 mg/ml
VmLNBs 1 mg/ml
NBs
Log (CFUs/ml)
Incubation time
2 h
3 h
4 h
6 h
24 h
B
Ctr
Vm 0.1 mg/ml
VmLNBs 0.1 mg/ml
NBs
Log (CFUs/ml)
incubation time
C
Ctr
Vm 0.01 mg/ml
VmLNBs 0.01 mg/ml
NBs
Log (CFUs/ml)
Incubation time
D
Ctr
Vm 0.004 mg/ml
VmLNBs 0.004 mg/ml
NBs
Log (CFUs/ml)
Incubation time

Figure 7

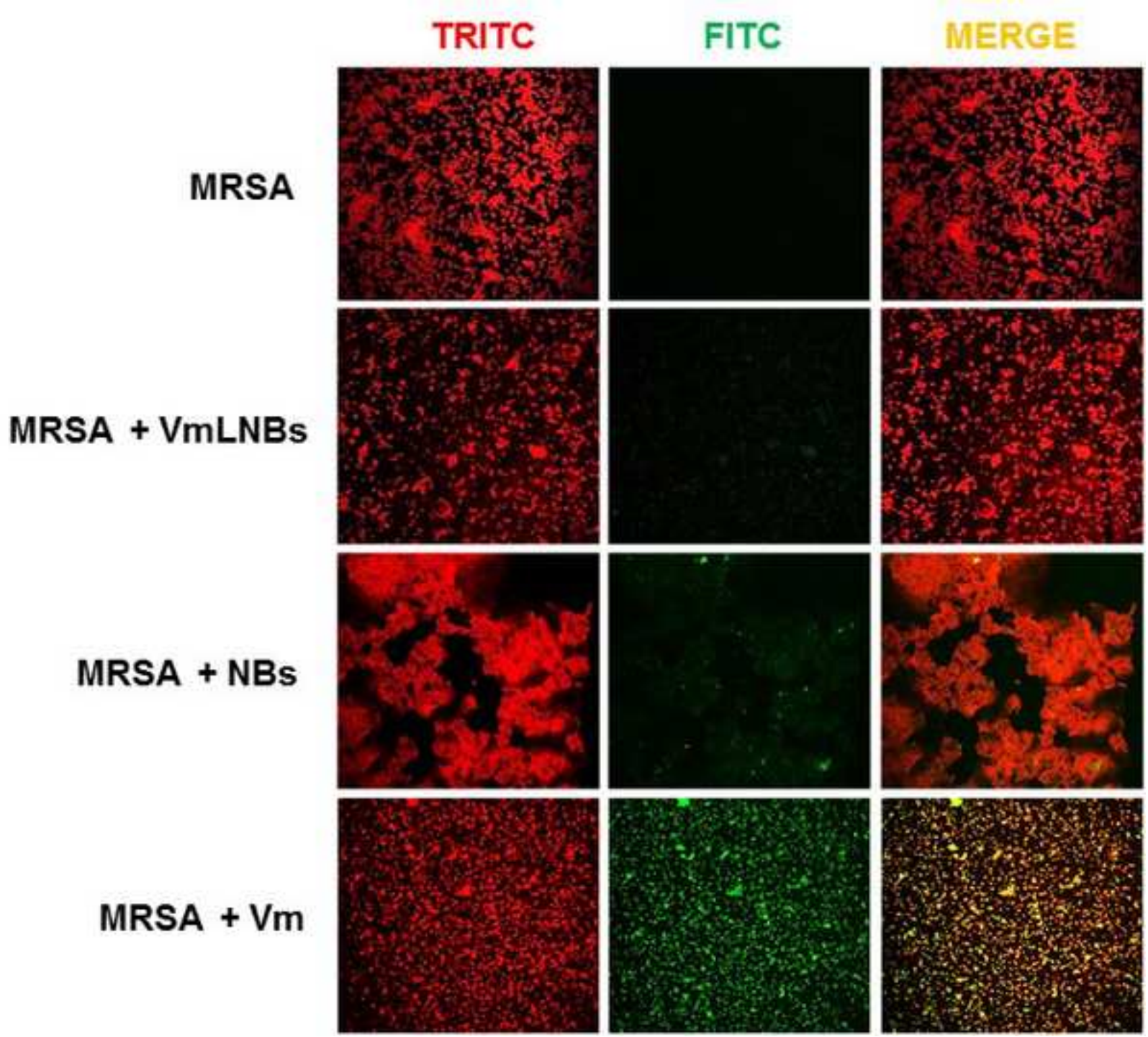

Figure 8

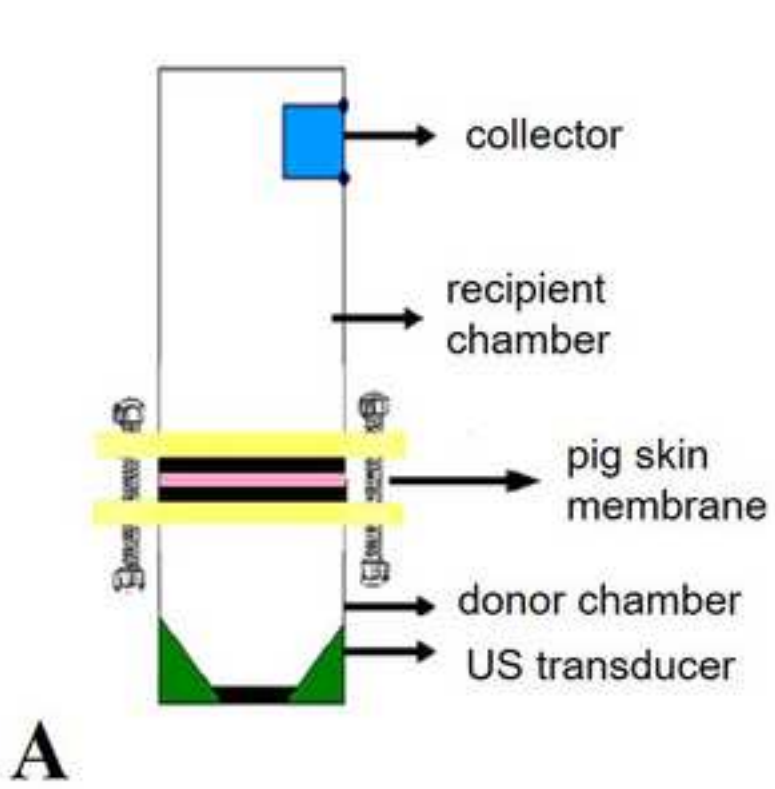
collector
recipient chamber
pig skin membrane
donor chamber
US transducer

A

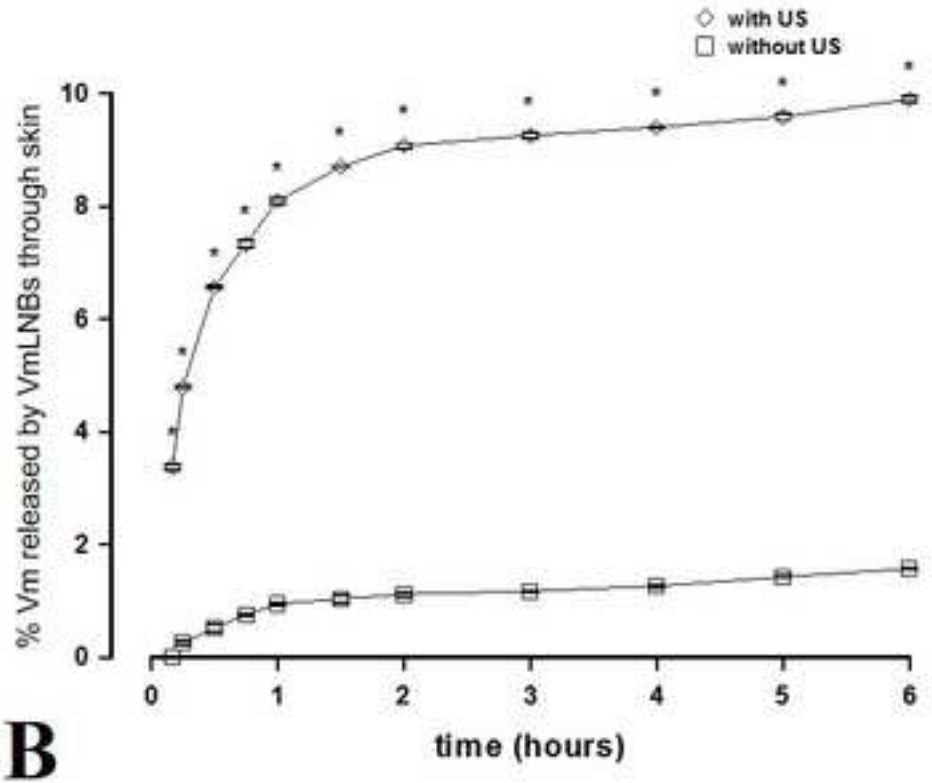
with US
without US
% Vm released by VmLNBs through skin
time (hours)
0
2
4
6
8
10
0
1
2
3
4
5
6

B

Supplementary Material (clean copy)

Click here to download Supplementary Material: Argenziano et al Int J Pharm 2017 SUPPL MAT revised (CLEAN COPY).doc

Supplementary Material (marked copy)

Click here to download Supplementary Material: Argenziano et al Int J Pharm 2017 SUPPL MAT revised (MARKED COPY).doc